DMD Fast Forward. Published on March 5, 2014 as doi:10.1124/dmd.113.056341




# Metabolism and Pharmacokinetics of Allitinib in Cancer Patients: the Roles of Cytochrome P450s and Epoxide Hydrolase in its Biotransformation

**Lishan Lin, Cen Xie, Zhiwei Gao, Xiaoyan Chen and Dafang Zhong**

Shanghai Institute of Materia Medica, Chinese Academy of Sciences, Shanghai, China (L. L., C. X., Z. G., X. C., D.Z.)

**Running Title:** Metabolism of allitinib in humans

**Corresponding Author:**

Dr. Dafang Zhong, Shanghai Institute of Materia Medica, Chinese Academy of Sciences, 501 Haike Road, Shanghai 201203, P.R. China

Tel/Fax: +86-21-50800738

E-mail: dfzhong@simm.ac.cn

Statistics:

Number of body text pages: 27

Number of tables: 5

Number of figures: 9

Number of references: 29

Number of words in the Abstract: 242

Number of words in the Introduction: 621

Number of words in the Discussion: 1359

DMD Fast Forward. Published on March 5, 2014 as DOI: 10.1124/dmd.113.056341
This article has not been copyedited and formatted. The final version may differ from this version.



**Abbreviations:**

ABT, 1-aminobenzotriazole; AUC: area under the concentration–time curve; CE, collision energy; $C_{max}$, maximum concentration; CYP, cytochrome P450; DMSO, dimethyl sulfoxide; ER, efflux ratio; HIM, human intestinal microsomes; HLM, human liver microsomes; HPM, human pulmonary microsomes; EGFR, epidermal growth factor receptor; HBSS, Hank's balanced salt solution; GSH, glutathione; GST, glutathione-S-transferase; KET, ketoconazole; LC-MS/MS, liquid chromatography–tandem mass spectrometry; M1, *O*-dealkylallitinib; M2, *O*-dealkyl-27,28-dihydrogenated allitinib; M5, *O*-dealky-27,28-dihydrodiol allitinib; M6, metabolite of amide hydrolysis; M10, 27,28-dihydrodiol allitinib; MDF, mass defect filtering; α-NF, α-naphthoflavone; NMR, nuclear magnetic resonance; $P_{app}$, apparent permeability coefficient; SIMM, Shanghai Institute of Materia Medica; $t_{max}$, time to the maximum concentration; UHPLC/Q-TOF MS, ultra-high performance liquid chromatography/quadrupole time-of-flight mass spectrometry.

DMD Fast Forward. Published on March 5, 2014 as DOI: 10.1124/dmd.113.056341
This article has not been copyedited and formatted. The final version may differ from this version.



**Abstract**

Allitinib, a novel irreversible selective inhibitor of the epidermal growth factor receptor 1 (EGFR) and human epidermal receptor 2 (ErbB2), is currently in clinical trials in China for the treatment of solid tumors. It is a structural analog of lapatinib but has an acrylamide side chain. Sixteen metabolites of allitinib were detected by ultra-high-performance liquid chromatography/quadrupole time-of-flight mass spectrometry. The pharmacologically active α,β-unsaturated carbonyl group was the major metabolic site. The metabolic pathways included *O*-dealkylation, amide hydrolysis, dihydrodiol formation, hydroxylation, and secondary phase II conjugation. The metabolite of amide hydrolysis (M6) and 27,28-dihydrodiol allitinib (M10) were the major pharmacologically active metabolites in the circulation. The steady-state exposure to M6 and M10 was 11% and 70% of that of allitinib, respectively. The biotransformation of allitinib was determined using microsomes and recombinant metabolic enzymes. In vitro phenotyping studies demonstrated that multiple cytochrome P450 (CYP) isoforms, mainly CYP3A4/5 and CYP1A2, were involved in the metabolism of allitinib. Thiol conjugates (M14 and M16) and dihydrodiol metabolites (M5 and M10) were detected in humans, implying the formation of reactive intermediates. The formation of a glutathione conjugate of allitinib was independent of NADPH and CYP, but was catalyzed by glutathione-S-transferase. CYP enzymes and epoxide hydrolase were involved in M10 formation. Overall, our study showed that allitinib was metabolized by the *O*-dealkylation pathway similar to lapatinib, but that amide hydrolysis and the formation of dihydrodiol were the dominant metabolic pathways. The absorbed allitinib was extensively

DMD Fast Forward. Published on March 5, 2014 as DOI: 10.1124/dmd.113.056341
This article has not been copyedited and formatted. The final version may differ from this version.



metabolized by multiple enzymes.

DMD Fast Forward. Published on March 5, 2014 as DOI: 10.1124/dmd.113.056341
This article has not been copyedited and formatted. The final version may differ from this version.



## Introduction

The ErbB family of receptor tyrosine kinases comprises four members, including epidermal growth factor receptor (EGFR), ErbB2, ErbB3 and ErbB4 (Klapper et al., 2000; Olayioye et al., 2000). Activation of these receptor tyrosine kinases plays important roles in the proliferation, survival, adhesion, migration, and apoptosis of cells. ErbB2 is predominantly existed in an active conformation for lack of any known endogenous ligands, and prevents the degradation of EGFR. Because of these features, ErbB2 has attracted increasing attention in recent years (Garrett et al., 2003; Xie et al., 2011). Abnormal expression of these receptors is related to the development and migration of tumors (Gonzales et al., 2008). Thus, the ErbB family of receptor tyrosine kinases is an important therapeutic target for the design of anticancer drugs.

Lapatinib (Tykerb®, GlaxoSmithKline, Brentford, Middlesex, UK), a 4-anilinoquinazolie derivative, is an orally administered small-molecule reversible inhibitor of EGFR and ErbB2. Lapatinib blocks the phosphorylation and activation of these receptors to prevent downstream signaling events by binding to the ATP-binding site of protein kinases and competing with the ATP substrate (Shewchuk et al., 2000). Although the safety profile of lapatinib is acceptable when treating breast cancer (Bence et al., 2005; Burris et al., 2005; Geyer et al., 2006), hepatotoxicity has been reported in some patients treated with lapatinib (Peroukides et al., 2011).

Allitinib (AST1306; *N*-(4-(4-(3-fluorobenzyloxy)-3-chlorophenylamino)quinazolin-6-yl) acrylamide), is a novel analog of lapatinib. In contrast to lapatinib, it is an irreversible inhibitor of EGFR and

DMD Fast Forward. Published on March 5, 2014 as DOI: 10.1124/dmd.113.056341
This article has not been copyedited and formatted. The final version may differ from this version.



ErbB2. Allitinib is currently being evaluated in clinical trials in China for the treatment of solid tumors. Unlike other known irreversible EGFR and ErbB2 inhibitors, such as HKI-272 (Rabindran et al., 2004), BIBW2992 (Eskens et al., 2008; Takezawa et al., 2010; Yap et al., 2010) and PF-00299804 (Gonzales et al., 2008), allitinib is more effective in ErbB2-dependent models than in EGFR-dependent models. Compared with lapatinib, allitinib is associated with greater inhibition of EGFR and ErbB2. After incubation of allitinib at different concentrations with kinases at 37°C for 1 h, allitinib exhibited $IC_{50}$ values of 0.5 nM and 3.0 nM towards EGFR and ErbB2, respectively. Furthermore, allitinib shows inhibitory activity against mutant forms of EGFR. Animal studies have also demonstrated that allitinib potently inhibits tumor growth in human tumor xenograft mouse models (Xie et al., 2011).

The α,β-unsaturated carbonyl group of allitinib was pharmacologically designed to covalently bind to cysteine residue Cys797 in EGFR and to Cys805 in ErbB2 via Michael addition (Xie et al., 2011). However, because this α,β-unsaturated carbonyl group is electrophilic, allitinib might covalently bind to proteins and other nucleophilic biomolecules, with potentially adverse effects. To evaluate the pharmacology and safety of new drugs, it is necessary to determine their disposition and metabolism during the clinical development program. In particular, the metabolites of new drugs might contribute to their pharmacological or toxicity profiles in vivo (Baillie et al., 2002). The pharmacokinetics, metabolism, and disposition of allitinib have been investigated in rats (data not shown). Allitinib was absorbed quickly, and the maximum concentration ($C_{max}$) was achieved at 1.0–3.0 h after administration. Its concentration decreased quickly with $t_{1/2}$ of 3.4–4.4 h.

DMD Fast Forward. Published on March 5, 2014 as DOI: 10.1124/dmd.113.056341
This article has not been copyedited and formatted. The final version may differ from this version.



Systemic available allitinib was extensively metabolized to thiol conjugates and dihydrodiol metabolites, which indicated that allitinib tended to form reactive intermediates. The bioavailability of allitinib was only 5.7% in rats, which might be related to (1) poor solubility, (2) first-pass metabolism, (3) poor permeability, (4) efflux transport.

The objectives of the current study were as follow: (1) to characterize the metabolic pathways of allitinib in cancer patients at the steady state following its repeated oral administration; (2) to determine the pharmacokinetic profile and routes of excretion of allitinib; and (3) to explore the mechanisms involved in the formation of the major metabolites in vitro to understand the metabolism of the acrylamide group.

## Materials and Methods

**Chemicals.** Reference standards of allitinib (99.7% purity), NB-2 ((E)-*N*-(4-((3-chloro-4-((3-fluorobenzyl)oxy)phenyl)amino)quinazolin-6-yl)but-2-enamide, 96% purity), *O*-dealkyl-27,28-dihydrogenated allitinib (M2), and the metabolite of amide hydrolysis (M6) were supplied by Allist Pharmaceuticals Inc. (Shanghai, China). The metabolites *O*-dealkylallitinib (M1), *O*-dealky-27,28-dihydrodiol allitinib (M5), 27,28-dihydrodiol allitinib (M10) and allitinib epoxide (M23) were synthesized and purified in our laboratory. Pooled mixed-gender human liver microsomes, pooled mixed-gender human liver cytosol, pooled mixed-gender human intestinal microsomes, pooled mix-gender human pulmonary microsomes, and recombinant CYP enzymes (CYP1A2, CYP1B1, CYP2A6, CYP2B6, CYP2C8, CYP2C9, CYP2C19, CYP2D6, CYP2E1, CYP3A4, CYP3A5, and CYP4A11) were purchased from BD Gentest (Woburn, MA). Caco-2 cells at passage 17 were purchased from the American Type Culture Collection (Rockville, MD). β-Glucuronidase, sulfatase, 1-aminobenzotriazole (ABT), α-naphthoflavone (α-NF), sulfaphenazole, ticlopidine, quinidine, clomethiazole, ketoconazole (KET), quercetin, Hank's balanced salt solution (HBSS) and cell-culture reagents were acquired from Sigma-Aldrich (St. Louis, MO). All solvents were of analytical or high-performance liquid chromatography (HPLC) grade. Purified water was generated with a Milli-Q Gradient Water Purification System (Millpore, Molsheim, France).

**Clinical Study Design.** The study was performed at Fudan University Shanghai Cancer Center (Shanghai, China) and was approved by the Ethics Committee of Fudan

DMD Fast Forward. Published on March 5, 2014 as DOI: 10.1124/dmd.113.056341
This article has not been copyedited and formatted. The final version may differ from this version.



University Shanghai Cancer Center. All subjects gave their written informed consent before enrolment. Three Chinese cancer patients (two males and a female) were given 1000 mg of allitinib tosylate t.i.d. orally for 21 consecutive days. Blood samples were collected in heparinized tubes at the following time on days 1 and 24: before and at 0.5, 1, 1.5, 2, 3, 4, and 6 h after the first dose; before and and at 1, 2, 3, 4, 5, and 6 h after the second dose; before and at 1, 2, 3, 4, 8, 12, 24, and 36 h after the third dose. Additional samples were obtained before and 2 h after the dose on days 10 and 23. Plasma samples were separated and stored at −20 °C until analysis. Fecal samples were collected on days 10–12. The total fecal weight was recorded at the end of each collection interval. Five volumes of acetonitrile–water (2:1, *v*/*v*) were added to each fecal sample. The mixture was blended by a motor-driven homogenizer, and then vibrated by ultrasound wave for 30 min. A 50 mL aliquots of the mixture was removed and centrifuged at 3,500 × *g* for 5 min to produce fecal homogenate.

Another 10 subjects received a single oral dose of 1000 mg of allitinib tosylate. Urine samples were collected before and at 0–6, 6–12, 12–24, 24–48, and 48–72 h intervals after the start of oral administration. The total urine volume was recorded at each collection interval. The fecal homogenate and urine samples were stored at −20 °C until analysis.

**Metabolite Profiling of Human Plasma, Urine, and Fecal Samples.** *Sample Preparation*. Representative pooled plasma, urine, and fecal samples were prepared for metabolite profiling and identification experiments. Plasma samples taken at 0 h on day 1, and at 2, 4, and 6 h after the third dose on day 24 were pooled using equal volumes (100 μl) from each individual sample. Urine samples collected from 0–24 h were pooled across all

DMD Fast Forward. Published on March 5, 2014 as DOI: 10.1124/dmd.113.056341
This article has not been copyedited and formatted. The final version may differ from this version.



subjects by combining volumes proportional to the total volume excreted by each subject in each collection interval. Three volumes of acetonitrile were added to each plasma and urine sample. After vortex mixing and centrifugation at 11,000 × *g* for 5 min, the supernatant was transferred into a clean plastic tube and evaporated to dryness under a stream of air at 40 °C. The residues of the plasma and urine samples were reconstituted in 100 μl of 90% aqueous acetonitrile (*v*/*v*). Then, 10 μL of the reconstituted solution was injected into an ultra high-performance liquid chromatograph coupled to a quadrupole-time of flight-mass spectrometer (UHPLC/Q-TOF MS) system for analysis. Fecal samples were pooled by combining volumes proportional to the total volume of each fecal homogenate from all subjects. The pooled fecal homogenates were directly injected into the UHPLC/Q-TOF MS system for analysis.

**Enzyme Hydrolysis.** Pooled human urine samples were incubated with sulfatase and β-glucuronidase in 1 M citrate buffer (pH 5.0) in a water bath at 37°C for 16 h. The mixtures were treated as described above and analyzed.

**Synthesis of M1.** Allitinib was stirred with aluminum chloride in acetone at room temperature for 10 h. The mixture was then separated on a YMC-Pack ODS column (250 × 10 mm I.D., 5 μM; YMC Company Ltd., Kyoto, Japan) to obtain pure M1.

**Synthesis of M5 and M10.** M1 and citric acid (0.2 molar equivalent) were dissolved in acetone/water (5:1, *v*/*v*) in a 100 mL round-bottom flask. Potassium osmate (0.2 molar equivalent) was then added, followed by 4-methyl-morpholin *N*-oxide (1.1 molar equivalent). The mixture was stirred at room temperature for 48 h and quenched by the addition of sodium hyposulfite. Acetone was removed by placing the flask on a rotary

DMD Fast Forward. Published on March 5, 2014 as DOI: 10.1124/dmd.113.056341
This article has not been copyedited and formatted. The final version may differ from this version.



evaporator. The aqueous residue was extracted with ethyl acetate and separated on a YMC-Pack ODS column (250 × 10 mm I.D., 5 μM; YMC Company Ltd.) to yield pure M5. The M10 synthetic standard was acquired with the same chemical reaction after replacing M1 with allitinib.

**Synthesis of Allitinib Epoxide.** Allitinib tosylate (0.18 mmol) was dissolved in 3.75 mL formic acid, and 2 mL $H_2O_2$ was added. The content was heated at 45 °C for 3 h. After adding two volumes of acetonitrile-water (2: 1, *v*/*v*) and adjusting the pH value to 3 with 1% ammonia, the mixture was then separated on a Shim-Pack PREP-ODS(H) KIT column (250 × 20 mm I.D., 5 μM; Shimadzu, Kyoto, Japan) to yield pure allitinib epoxide.

**Pharmacokinetic Analysis.** The pharmacokinetic characteristics of allitinib, M6 and M10 were analyzed using the noncompartmental model with Winnonlin 5.3 software (Pharsight, Mountain View, CA). The $C_{max}$ and the time to reach the maximum concentration ($t_{max}$) were directly determined from the experimental data. The linear–log trapezoidal method was used to calculate the area under the plasma concentration–time curve for 0–24 h ($AUC_{0-24\,h}$). The accumulation ratio (day 24/day1) for $AUC_{0-24}$ was also calculated. The elimination rate constant ($k_e$) was determined by least squares regression of the terminal log–linear phase of the concentration–time curve. The terminal half-life was estimated as $\ln 2/k_e$.

**In Vitro Pharmacological Activity of the Metabolites of Allitinib.** The inhibitory activities of M1, M6, and M10 against EGFR and ErbB2 were determined as previously described (Xie et al., 2011).

**Microsomal Incubation.** A stock solution of allitinib was prepared in dimethyl

DMD Fast Forward. Published on March 5, 2014 as DOI: 10.1124/dmd.113.056341
This article has not been copyedited and formatted. The final version may differ from this version.



sulfoxide (DMSO). A mixture containing 1 μM allitinib was mixed with microsomes (human liver microsomes (HLM), human intestinal microsomes (HIM), and human pulmonary microsomes (HPM), 1 mg/mL), and phosphate–buffered saline (PBS; 100 mM, pH 7.4) without or with 1 mM glutathione (GSH) at a final volume of 200 μL. The final DMSO concentration was 0.1%. After preincubation at 37 °C for 3 min, 1 mM NADPH was added to initiate the reaction. After incubation for 60 min, two volumes of ice-cold acetonitrile were added to terminate the reaction. Control samples without NADPH or microsomes were also prepared. To evaluate the contribution of glutathione transferase (GST) to the formation of the reactive metabolites, separate samples were prepared with 1 mg/mL human liver cytosol (HLC), 1 μM allitinib and 1 mM GSH. Each incubation was performed in duplicate. After the samples were centrifuged at 11,000 × *g*, the supernatants were evaporated to dryness under an air stream at 40 °C. The residues were reconstituted in 100 μL water/acetonitrile (90:10, *v*/*v*). Then, 10 μL aliquot of the reconstituted solution was injected into the UHPLC/Q-TOF MS system for analysis.

**Identification of CYP Enzymes Involved in the Metabolism of Allitinib**. A stock solution of allitinib was prepared in DMSO. Allitinib (1 μM) was incubated in the presence of individually expressed recombinant CYP enzymes (50 pmol/mL 1A2, 1B1, 2A6, 2B6, 2C8, 2C9, 2C19, 2D6, 2E1, 3A4, 3A5, or 4A11 suspended in 100 mM PBS, pH 7.4) and 2 mM NADPH at 37 °C for 60 min. The final DMSO concentration during incubation was 0.1%. Two volumes of ice-cold acetonitrile containing an internal standard (500 ng/mL NB-2) were added to terminate the reaction. A sample incubated without NADPH was used as the negative control.

DMD Fast Forward. Published on March 5, 2014 as DOI: 10.1124/dmd.113.056341
This article has not been copyedited and formatted. The final version may differ from this version.



**Inhibition of the Oxidative Metabolism of Allitinib by Selective P450 Inhibitors.** To evaluate the relative contributions of different microsomal enzyme systems to the metabolism of allitinib in HLM, 1 μM allitinib was incubated at 37 °C for 60 min with 1 mg/mL HLM alone or in the presence of different chemical inhibitors of CYP, including the non-specific CYP inhibitor 1-aminobenzotriazole (ABT; 1 mM), the specific CYP1A1/2 inhibitor *α*-NF (2 μM), the CYP2C8 inhibitor quercetin (1 μM), the CYP2C9 inhibitor sulfaphenazole (6 μM), the CYP2B6/2C19 inhibitor ticlopidine (0.4 μM), the CYP2D6 inhibitor quinidine (2 μM), the CYP2E1 inhibitor clomethiazole (0.1 μM), or the CYP3A4/5 inhibitor KET (1 μM). After incubation, two volumes of ice-cold acetonitrile containing NB-2 were added to terminat the reaction. Each incubation was performed in duplicate.

The MS peak area ratios of allitinib and the detected metabolites to the internal standard in each incubation system were recorded to determine the contributions of the CYP enzymes to the metabolism of allitinib. The results were compared with those for control samples lacking the inhibitors.

**Mechanism of M10 Formation**. Valpromide (10, 100, or 1000 μM), an inhibitor of epoxide hydrolase, was preincubated with HLM and NADPH for 3 min. Allitinib was added to the mixture to a final volume of 200 μL. A control sample without valpromide was also prepared. Each incubation was performed in duplicate. After incubation for 60 min, two volumes of ice-cold acetonitrile were added to terminate the reaction. After protein precipitation, the supernatant was evaporated to dryness at 40°C under a gentle stream of air. The residue was reconstituted in 80.0 μL of 90% aqueous acetonitrile (*v*/*v*).

DMD Fast Forward. Published on March 5, 2014 as DOI: 10.1124/dmd.113.056341
This article has not been copyedited and formatted. The final version may differ from this version.



The MS peak area ratios of M10 to epoxide in each incubation system were recorded to determine the role of valpromide in the formation of M10. The results were compared with those for control samples lacking valpromide.

**Incubation of Allitinib Epoxide in HLC.** Stock solution of allitinib epoxide were prepared in DMSO. The allitinib epoxide (20 nM or 2 μM) was incubated with 1 mg/mL HLC, GSH (2 mM), magnesium chloride (5 mM), EDTA (0.1 mM), and PBS (100 mM, pH 7.4). The final DMSO concentration during incubation was 0.1%. The incubation was conducted in duplicate at 37 °C in a total volume of 200 μL.The reaction was terminated after 60 min of incubation by adding two volumes of ice-cold acetonitrile. Control samples without HLC were also prepared. After protein precipitation, the supernatant was evaporated to dryness at 40°C under a gentle stream of air. The residue was reconstituted in 100 μL of 90% aqueous acetonitrile (*v*/*v*). A aliquot of 10 μL of the reconstituted solution was injected into the UHPLC/Q-TOF MS for analysis.

**Caco-2 Cell Permeability Study**. For the cell permeability experiments, Caco-2 cells were seeded in 24-well inserts at a density of $10^5$ cells/cm$^2$ to generate Caco-2 monolayers. The cells were cultured for 21 days, during which time the medium was replaced every three days. Cell layers with a transepithelial electrical resistance value > 300 Ω·cm$^2$ were used in the permeability experiment. Before the assay, the monolayers were gently washed twice with warm HBSS (pH 7.4, 37 °C). HBSS containing 2 μM allitinib was added to the apical side (150 μL) or the basolateral side (750 μL) of the inserts to initiate the experiment. The cells were then incubated at 37 °C for 2 h in a humidified atmosphere containing 5% $CO_2$. Next, 200 μL of transport buffer was collected from the apical or

DMD Fast Forward. Published on March 5, 2014 as DOI: 10.1124/dmd.113.056341
This article has not been copyedited and formatted. The final version may differ from this version.



basolateral side and mixed with the same volume of methanol. HBSS containing allitinib at the donor side was collected before and after the assay to calculate assay recovery. After washing three times, cell monolayers were lysed with 200 μL acetonitrile. All incubations were performed in triplicate. The concentration of allitinib was analyzed by LC-MS/MS.

The apparent permeability coefficients ($P_{app}$, cm/s) were calculated with the following equation:

$$P_{app}=\frac{\Delta Q}{\Delta t}\times\frac{1}{A\times C_{donor}}$$

where $\Delta Q/\Delta t$ is the rate of permeability (nmol/s), A is the surface area of the insert ($cm^2$), and $C_{donor}$ is the initial concentration on the donor side (nmol/mL).

The efflux ratio (ER) was determined as follows:

$$ER=\frac{P_{app(B-A)}}{P_{app(A-B)}}$$

where $P_{app(A-B)}$ and $P_{app(B-A)}$ represent the apparent permeability coefficients of the substrate from the apical to the basolateral side and from the basolateral to the apical side, respectively.

**Analytical Conditions**. *Metabolite Profiling by UHPLC-UV/Q-TOF-MS*. Metabolic profiling of allitinib in biological samples was performed on a Waters Acquity UHPLC system (Waters, Milford, MA) equipped with a binary solvent delivery pump, column oven, UV detector and autosampler. Chromatographic separation was performed on an Acquity UPLC HSS T3 column (100 × 2.1 mm I.D., 1.8 μm; Waters) at 40 °C. The mobile phase was a mixture of 5 mM ammonium formate in water containing 0.05% formic acid (A) and acetonitrile (B) at a flow rate of 0.4 mL/min. Elution started with 1 min isocratic run with 10% solvent B, followed by a linear gradient of 10% to 55% solvent B in 14 min, 55% to

DMD Fast Forward. Published on March 5, 2014 as DOI: 10.1124/dmd.113.056341
This article has not been copyedited and formatted. The final version may differ from this version.



99% solvent B in 1 min, maintained for 1 min, and then reduced to 10% B to equilibrate the column. The eluate was monitored by ultraviolet (UV) detection at 300 nm.

For metabolite profiling, MS detection was conducted with a Synapt Q-TOF high-resolution mass spectrometer (Waters) in the positive electrospray ionization mode. Nitrogen and argon were used as the desolvation and collision gases, respectively. The capillary and cone voltage were set at 3000 and 40 V, respectively. Data from 80 to 1000 Da were acquired using a source temperature of 120 °C and a desolvation temperature of 350 °C. Data were corrected during acquisition using a reference (LockSpray®) sample comprising 400 ng/mL leucine encephalin (*m/z* 556.277) infused at 20 μL/min. An $MS^E$ with two separate scan functions programmed with independent collision energies (CE) was used for data acquisition. At low CE, the transfer and trap CEs were 2 and 3 eV, respectively. At high CE, the transfer CE was 10 eV and the trap CE ranged from 10 to 20 eV. This mode of data collection allowed us to detect intact precursor ions and fragments.

Data processing was performed using a MetaboLynx subroutine of the MassLynx software (Waters). Mass defect filtering (MDF) was used to screen metabolites using a 40 mDa filter between the filter and the target metabolites. The fragment ion spectra were compared between the parent compound and the metabolites to help identify the metabolites, including the structure and site(s) of modification in the parent molecule.

To determine M23 in HLC incubation, MS detection was conducted on a triple TOF™ 5600+ MS/MS system (AB Sciex, Concord, Ontario, Canada) in the positive ESI mode. Mass range was set at *m/z* 100 – 1000. The following parameter settings were used: ion spray voltage: 5500 V; declustering potential: 80 V; ion source heater: 550 °C; curtain

DMD Fast Forward. Published on March 5, 2014 as DOI: 10.1124/dmd.113.056341
This article has not been copyedited and formatted. The final version may differ from this version.



gas: 40 psi; ion source gas 1: 55 psi; ion source gas 2: 55 psi. For TOF MS scans, collision energy (CE) was 10 eV; for product ion scans, CE was 55 eV, and collision energy spread (CES) was 10 in MS/MS experiment. Information-dependent acquisition (IDA) was used to trigger acquisition of MS/MS spectra for ions matching the IDA criteria. Real time Multiple Mass Defect Filter (MMDF) was used in IDA criteria.

*Quantitation of Allitinib and its Metabolites in Plasma with LC-MS/MS*. The concentrations of allitinib, M6, and M10 were quantified simultaneously using a previously described LC-MS/MS method (Lin et al., 2013).

*Quantification of M1 in Urine with LC-MS/MS*. The LC system consisted of two LC-20ADXR pumps and a SIL-20ACXR autosampler (Shimadzu, Kyoto, Japan). A TSQ Quantum Vantage triple-quadrupole MS (Thermo Fisher Scientific, Waltham, MA) equipped with a positive electrospray ionization source was used for MS detection. Selected-reaction monitoring (SRM) was used to detect the analyte and internal standard. The MRM transitions *m/z* 341.0 → *m/z* (251.0 + 277.0 + 285.0 + 305.0) and *m/z* 587.0 → 167.0 were used to detect M1 and irinotecan, respectively.

The concentration of M1 in urine was determined using a validated LC-MS/MS method. After incubating equal volumes of β-glucuronidase (2000 units of type HA-4; Sigma-Aldrich) and sulfatase (15 units of Type VIII; Sigma-Aldrich) in 1 M citrate buffer (pH 5.0) at 37 °C for 16 h, M1 and the internal standard, irinotecan, were separated on a Gemini $C_{18}$ column (50 × 2.0 mm I.D., 5 μm; Phenomenex, Torrance, CA). The mobile phase was 10 mM ammonium acetate containing 0.1% formic acid mixed with methanol containing 0.1% formic acid (60:40, *v*/*v*).

DMD Fast Forward. Published on March 5, 2014 as DOI: 10.1124/dmd.113.056341
This article has not been copyedited and formatted. The final version may differ from this version.



*Quantification of Allitinib and its Metabolites in Feces by HPLC-UV.* An Agilent 1260 HPLC system (Agilent) was used to determine the concentrations of allitinib and its major metabolites (M2, M5, M6, and M10) in fecal samples. An ASB $C_{18}$ column (150 × 4.6 mm I.D., 5 μm; Agela Technologies, Wilmington, DE) was used to separate Allitinib, M2, M5, M6, M10, and NB-2 (internal standard). The mobile phase consisted of a mixture of 0.1% formic acid in methanol (A) and 0.1% formic acid in 10 mM ammonium acetate (B). Gradient elution was initiated at 40% A, maintained for 5 min, and then increased to 70% A in 2 min, which was maintained for 5 min. The elution was then increased to 80% A in 1 min, maintained for 5 min, and immediately decreased to 40% A to equilibrate the column. The flow rate was set at 1 mL/min, and a wavelength of 380 nm was used to monitor the analytes.

DMD Fast Forward. Published on March 5, 2014 as DOI: 10.1124/dmd.113.056341
This article has not been copyedited and formatted. The final version may differ from this version.



## Results

**MS Fragmentation Behavior of Allitinib.** The metabolites of allitinib were identified by comparing their chromatographic and MS fragmentation behaviors with those of the parent drug and the synthesized reference standards. We first examined the chromatographic and MS fragmentation behaviors of the reference allitinib. Allitinib was eluted at 14.1 min and a protonated molecule $[M+H]^+$ was detected at *m/z* 449.120 in the positive ion mode. The high CE MS (Fig. 1A) yielded fragment ions at *m/z* 340.074, 339.069, 313.054 (100% abundance), 311.074, 305.109, 287.071, 277.107, and 213.081. The predominant ion at *m/z* 313.054 was formed via the loss of terminal olefin and cleavage of the alkyl C–O bond. The radical ion at *m/z* 340.074 formed from the hemolysis of the alkyl C–O bond, which was followed by the loss of a specific 109 Da moiety (1-fluoro-3-toluene free radical), while *m/z* 339.069 was proposed to form from the cleavage of alkyl C–O bond. The ions at *m/z* 311.074, 305.109, 287.071, 277.107, and 213.081 formed from the cleavage of *N*-(4-((3-chloro-4-hydroxyphenyl)amino)quinazolin-6-yl)acrylamide. According to the fragmentation pattern, the structure of allitinib was divided into segments A, B, and C (Fig. 1B). The structures of the metabolites were characterized by determining the changes in the *m/z* values of these three segments.

A total of 11, 12, and 10 metabolites of allitinib were detected in human plasma, urine, and feces, respectively (Fig. 2 and Fig. 3). The metabolites were designated as M0 (parent compound, allitinib) to M16 based on their *m/z* values. According to the UV chromatograms, the major components in plasma were M0 followed by M6 and M10,

DMD Fast Forward. Published on March 5, 2014 as DOI: 10.1124/dmd.113.056341
This article has not been copyedited and formatted. The final version may differ from this version.



whereas those in urine were M1 and its glucuronide conjugate, M13. M0 was the predominant compound in feces, whereas M2 and M6 were relatively minor. Table 1 lists the characteristics of the possible metabolites of allitinib, including their retention times and proposed elemental compositions, and their characteristic fragment ions. The proposed metabolic pathways of allitinib in humans are shown in Fig. 4. The information used to assign each metabolite is summarized in the Supplementary Results. The detection of cysteine conjugates and dihydrodiol metabolites in plasma suggested the formation of reactive intermediates. The structures of M1, M2, M5, M6, and M10 were confirmed by comparing their chromatographic retention times and the mass spectra with those of reference standards. The $^{1}$H-nuclear magnetic resonance (NMR) data for the reference standards are listed in Table 2.

**Pharmacokinetics and Excretion of Allitinib.** The concentrations of allitinib, M6, and M10 in human plasma were quantified after the oral administration of 1000 mg of allitinib tosylate t.i.d. for 21 consecutive days. The pharmacokinetic characteristics of allitinib, M6, and M10 are listed in Table 3. The $C_{max}$ values for allitinib, M6, and M10 were achieved at 3.6–5.2 h after the first dose. The $AUC_{0\text{-}24}$ values for M6 and M10 was 14% and 65% of that to the parent drug (based on molar concentrations), respectively. After the last dose, the $C_{max}$ values for allitinib, M6, and M10 were achieved at approximately 2.5–3.2 h. At steady state, the terminal half-lives of allitinib, M6, and M10 were observed at 4.5–9.9 h, at 6.3 h–15.8 h, and at 4.6–11.6 h, respectively. The $AUC_{0\text{-}24}$ values for M6 and M10 were 11% and 70% of that for the parent drug, respectively. The accumulation ratios of allitinib, M6, and M10 were 1.39–2.02, 1.06–2.78, and 0.74–2.43,

respectively.

At steady state, the daily fecal excretion of allitinib and its major metabolites M2, M5, and M6 accounted for 32.5% ± 17.4% of the dose. In the fecal samples, unchanged allitinib accounted for 30.4% ± 20.3% of the dose, whereas the major metabolites M2, M5, and M6 accounted for 1.41%, 0.067% and 0.635% of the dose, respectively. After a single oral dose of 1000 mg of allitinib tosylate, a combination of M1 and its glucuronide conjugate in urine accounted for 0.042% of the dose.

**In Vitro Pharmacological Activity of the Major Metabolites of Allitinib.** The results of in vitro pharmacological activity studies of the major metabolites are presented in Table 4. The results showed that M1, M6, and M10 were potent inhibitors of EGFR, but weak inhibitor of ErbB2.

**Microsomal Incubation.** After incubation with microsomes for 60 min, approximately 58% of the parent compound was consumed by HLM compared with 10% by HIM. Allitinib was not metabolized by HPM. Therefore, the liver was considered to be the major site of allitinib biotransformation.

Five metabolites were generated by incubating allitinib with HLM in the presence of NADPH. Based on the MS peak areas, the main metabolite in vitro was M5, followed by M1, M10, and M6. In samples lacking NADPH, only M6 was detected, which indicates that the formation of M1, M5, and M10 was NADPH-dependent, and that CYP enzymes played important roles in the formation of these metabolites. The formation of M6 was NADPH-independent, and amidohydrolase was assumed to be responsible for its formation. The properties of the metabolites identified after allitinib was incubated with HLM are

DMD Fast Forward. Published on March 5, 2014 as DOI: 10.1124/dmd.113.056341
This article has not been copyedited and formatted. The final version may differ from this version.



listed in Table 5.

**Identification of CYP Enzymes Involved in the Oxidative Metabolism of Allitinib.** In vitro studies were performed to identify which CYP enzymes were involved in the metabolism of allitinib and the formation of M1 and M10. As shown in Fig. 5, after 1 μM allitinib was incubated with recombinant CYP enzymes in the presence of NADPH, it was metabolized by 11 of the enzymes tested, but not CYP2C9. Based on the mean hepatic expression of the CYP enzymes (Rodrigues, 1999), the predominant enzyme involved in the metabolism of allitinib was CYP3A4, followed by CYP3A5 and CYP2C8. In the presence of NADPH, M1 was mainly produced by recombinant CYP3A4 and CYP2C8, followed by CYP2C19, CYP2E1 and CYP3A5, whereas M10 was mainly produced by CYP1A2, followed by CYP2D6 and CYP3A5.

To further determine the relative contribution of the different CYPs in allitinib biotransformation, ABT (non-specific CYP inhibitor), α-NF (CYP1A2 inhibitor), sulfaphenazol (CYP2C9 inhibitor), ticlopidine (CYP2B6/CYP2C19 inhibitor), quercetin (CYP2C8 inhibitor), quinidine (CYP2D6 inhibitor), clomethiazole (CYP2E1 inhibitor) and KET (CYP3A4/5 inhibitor) were individually added to HLM preparations. The results are presented in Fig. 6. The metabolism of allitinib was inhibited by all seven CYP inhibitors. The amount of allitinib that remained following incubation with ABT was approximately three times greater than that in the control group, suggesting that CYP enzymes played important roles in the oxidative metabolism of allitinib. The formation of M1 and M10 was markedly reduced in the presence of ABT, indicating that CYP enzymes were important in the production of M1 and M10. The formation of M1 were inhibited by 27.8% and 25.5%

in the presence of quinidine and KET, respectively. The formation of M10 were inhibited by 18.6% and 44.0% in the presence of α-NF and KET, respectively. These results indicated that CYP2D6 and CYP3A4/5 were the major enzymes involved in the formation of M1, whereas CYP3A4/5 was the predominant enzyme involved in the production of M10, followed by CYP1A2.

**Epoxide Hydrolase is Responsible for the Formation of M10.** It has been suggested that M10 is formed by CYP enzymes via an epoxide intermediate, and the resulting epoxide is hydrolyzed to M10 by epoxide hydrolase. To evaluate this possibility, HLM were incubated with valpromide, an epoxide hydrolase inhibitor, in the presence of NADPH. The coincubation of allitinib with valpromide resulted in the production of epoxide, which was eluted at 13.2 min. The protonated molecule of epoxide was detected at *m/z* 465.105, so was 16 Da larger than that of allitinib, indicating that an oxygen atom was introduced into allitinib. The ion at *m/z* 356.067 was formed by the loss of the pyroglutamic acid moiety (129 Da). The product ion at *m/z* 287.056 was identical to that of the parent drug, whereas the product ions at *m/z* 355.059, 327.064, 321.103, and 293.105 were 16 Da greater than those of the parent drug (*m/z* 339.069, 311.072, 305.109, and 277.103, respectively). These results suggested that an oxygen atom was probably attached to segment C of allitinib to form an epoxide. The identity of allitinib epoxide were further confirmed using synthetic standards.

As shown in Fig. 7, the formation of M10 decreased and the production of allitinib epoxide increased with increasing concentrations of valpromide. These results confirmed that epoxide hydrolase displayed an important role in the formation of M10.

DMD Fast Forward. Published on March 5, 2014 as DOI: 10.1124/dmd.113.056341
This article has not been copyedited and formatted. The final version may differ from this version.



**Mechanism Involved in Thiol Conjugate Formation.** Cysteine conjugates (M9 and M14) and *N*-acetyl cysteine conjugates (M12 and M16) were detected in humans, indicating the formation of reactive intermediates. To determine the mechanism involved in the formation of these thiol conjugates, in vitro studies were performed using GSH as a trapping agent. The coincubation of allitinib with GSH resulted in the production of a GSH conjugate, M22, which was determined as a major metabolite in rats after intravenous injection. It was eluted at 9.6 min. The protonated molecule of M22 was detected at *m/z* 756.206, and was 307.090 Da larger than that of allitinib, indicating the addition of a GSH molecule. Product ions were observed at *m/z* 627.163, 449.096, 341.092 and 287.073. The ion at *m/z* 627.163 resulted from the loss of the pyroglutamic acid moiety (129 Da). The product ions at *m/z* 341.092 and 287.073 were identical to those of the parent drug. These results suggested that the GSH molecule probably attached to segment C of allitinib by Michael addition.

M22 was also observed when allitinib was incubated without NADPH or HLM, implying that the formation of the GSH conjugate was independent of NADPH and CYP. The chromatographic peak of M22 increased when allitinib was incubated with human liver cytosol, indicating that the formation of M22 was catalyzed by GST. Cysteine conjugate M14 was also detected when allitinib was incubated with GSH, HLM, and NADPH, suggesting that the cysteine conjugates of allitinib in humans might partly be derived from GSH conjugates via the mercapturate pathway.

**In Vitro Metabolism of Allitinib Epoxide by HLC.** The coincubation of allitinib epoxide (2 μM) with GSH in HLC allowed the formation of M6, M10 and a GSH

DMD Fast Forward. Published on March 5, 2014 as DOI: 10.1124/dmd.113.056341
This article has not been copyedited and formatted. The final version may differ from this version.



conjugate, M23, which was eluted at 9.3 min. M23 exhibited $[M+H]^+$ ions at *m/z* 772.196, and was 307.083 Da larger than that of allitinib epoxide, suggesting the addition of a GSH molecule. The loss of pyroglutamic acid moiety resulted the formation of fragment ion at *m/z* 643.154. The product ions at *m/z* 355.062, 327.072 and 321.101 were identical to those of allitinib epoxide. These results suggested that the GSH molecule most likely attached to epoxy part. When a much lower substrate concentration (20 nM) was applied, M6 and M10 could be detected except M23 (Fig. 8).

**Caco-2 Cell Permeability Study.** The permeability of Caco-2 cells to allitinib was determined at a concentration of 2 μM. The $P_{app(A-B)}$ of allitinib was $0.77 \times 10^{-6}$ cm/s, indicating that the cells showed poor permeability to allitinib. When the transport of allitinib in the apical-to-basolateral was compared with that in the basolateral-to-apical directions, no apparent efflux transport was observed based on an ER of 1.40.

DMD Fast Forward. Published on March 5, 2014 as DOI: 10.1124/dmd.113.056341
This article has not been copyedited and formatted. The final version may differ from this version.



## Discussion

This study characterized the metabolic profiles of allitinib in cancer patients, and established its biotransformation mechanisms.

Allitinib was quickly absorbed, with a $t_{max}$ of approximately 3.0 h, consistent with the results of the preclinical study. Significant interpatient variability was observed after the oral administration of allitinib tosylate, indicating that dose modifications may be necessary to meet the individual patient's needs. The unmodified drug was the predominant substance detected in plasma. The amide hydrolysis metabolite (M6) and 27,28-dihydrodiol allitinib (M10) were the major pharmacologically active metabolites, accounting for approximately 11% and 70% of the estimated $AUC_{0-24}$ for the parent drug at steady state, respectively. The systemic clearance of M6 and M10 was slower than that of allitinib.

A total of 12 and 10 metabolites were identified in urine and feces, respectively. Unchanged allitinib was detected in trace amounts in urine, suggesting that the systemically available allitinib was metabolized extensively. The proposed structures of the metabolites M1, M2, M5, M6, and M10 were supported by comparisons with synthetic standards. The metabolic scheme of allitinib in humans is presented in Fig. 4 . The major metabolites in urine were *O*-dealkylallitinib (M1) and its glucuronide conjugate (M13). After the urine was incubated with β-glucuronidase and sulfatase for 16 h, the recovery of allitinib in terms of M1 was less than 0.1%, indicating that renal elimination makes a negligible contribution to the excretion of allitinib. After the oral administration of allitinib tosylate, the mean fecal excretion ratio was 32.5% ± 17.4% (range from 0.95% to 59.4%).

DMD Fast Forward. Published on March 5, 2014 as DOI: 10.1124/dmd.113.056341
This article has not been copyedited and formatted. The final version may differ from this version.



About 93.5% of the total fecal excretion was attributed to the unchanged drug. The major metabolite M2 accounted for 4.4% of the total fecal extraction, and the other two metabolites (M5 and M6) accounted for < 3.0%. The recovery of allitinib in fecal samples seemed to be related to the fecal weight excreted by the subjects. Several factors may contribute to the low recovery of allitinib in humans after its oral administration, including the difficulty in fully sampling the nonhomogeneously processed fecal samples, the loss of samples during collection or processing, or the covalent binding or non-covalent tissue uptake of the drug or its metabolites (Roffey et al., 2007). However, the results suggested that allitinib is predominantly eliminated via fecal excretion. To confirm this possibility, radiolabeled allitinib will be used in future mass balance experiments.

To further investigate the source of unchanged drug in feces, in vitro Caco-2 permeability study was performed. The result showed that the permeability of these cells to allitinib was poor ($P_{app} < 2.0 \times 10^{-6}$ cm/s). Thus, it might be concluded that the parent drug determined in human fecal samples was generated from the unabsorbed parent drug due to the poor bioavailability rather than excrected through biliary excretion after absorption.

The primary routes of allitinib biotransformation involved *O*-dealkylation (M1, M2, M3, M4, M5, M8, M9, M12, and M13), amide hydrolysis (M6), dihydrodiol formation (M5 and M10), and the subsequent phase II conjugation of these metabolites. The identified metabolic processes of lapatinib and allitinib are shown in Fig. 9, respectively. Allitinib shared several metabolic pathways with its analog lapatinib (Castellino et al., 2012), including the *O*-dealkylation and hydroxylation of the quinazoline moiety. However, the major metabolic sites of allitinib are located at the α,β-unsaturated carbonyl group, and

DMD Fast Forward. Published on March 5, 2014 as DOI: 10.1124/dmd.113.056341
This article has not been copyedited and formatted. The final version may differ from this version.



include amide hydrolysis and dihydrodiol formation. The formation of cysteine conjugate in vivo indicated that allitinib might covalently bind to proteins or biological macromolecules. The protein covalent binding ratios after incubation of allitinib with human plasma and HLM at 37 °C for 1 h were both less than 10.1%, and protein covalent binding of allitinib was time-dependent (data not shown). Further investigation is needed to obtain understanding of the impact of protein covalent binding on the potency of this drug. In vitro studies revealed that the reaction between allitinib and GSH was independent of microsomal CYP enzymes and NADPH, but that GST could catalyze the conjugation of allitinib and GSH.

In vitro metabolism studies using recombinant human CYP isozymes and inhibition studies using selective chemical inhibitors of CYP enzymes suggested that the oxidative metabolism of allitinib is mediated by multiple CYP enzymes. Allitinib was primarily metabolized by CYP3A4/5, followed by CYP1A2, CYP1B1, CYP2A6, CYP2B6, CYP2C8, CYP2C19, CYP2D6, CYP2E1 and CYP4A11. The formation of M1 was primarily mediated by CYP3A4/5 and CYP2D6, whereas CYP1A2 and CYP3A4/5 were mainly involved in the formation of M10. The incubation of allitinib with the CYP1A2 inhibitor α-NF in an HLM preparation markedly increased the production of M1, which was probably attributable to the stimulation role of CYP3A system by α-NF (Ueng et al., 1997; Maenpaa et al., 1998). Because multiple CYP enzymes were involved in the metabolism of allitinib, in vivo exposure to allitinib is unlikely to be markedly affected by CYP enzyme inhibitors. Therefore, the likelihood of drug–drug interactions mediated by the metabolism of allitinib is minimal.

DMD Fast Forward. Published on March 5, 2014 as DOI: 10.1124/dmd.113.056341
This article has not been copyedited and formatted. The final version may differ from this version.



The incubation of allitinib with HLM and valpromide, an inhibitor of epoxide hydrolase, confirmed that allitinib is metabolized to epoxide by CYP enzymes, and the epoxide metabolite is further metabolized to M10 by epoxide hydrolase. Epoxides can react with cellular macromolecules, such as DNA and protein, to exert mutagenic and genotoxic effects. Alternatively, GSH conjugates are produced by GST or dihydrodiol metabolites are produced by epoxide hydrolase to reduce their toxicity (Ehrenberg and Hussain, 1981; Hooberman et al., 1993; Faller et al., 2001; Lee et al., 2005; Gonzalez-Perez et al., 2012). The incubation of allitinib with HLM supplemented with NADPH and GSH confirmed that the pharmacologically active metabolite M10 was the major metabolite, but the GSH conjugate of epoxide M23 was not observed. M10 and M23 were both derived from allitinib epoxide. Our studies showed that allitinib epoxide could form a GSH conjugate at the concentration of 2 μM. However, when a much lower substrate concentration (20 nM) was used, the GSH conjugate at epoxide could not be detected, whereas the formation of M10 was observed, indicating that the epoxide intermediate was more readily metabolized to dihydrodiol than to the GSH conjugate.

An in vitro investigation showed that lapatinib was metabolized to *O*-dealkylated lapatinib by CYP3A4 and CYP2C8, and GSH and cysteinyl–glycine conjugates was also observed (Teng et al., 2010). Although allitinib was metabolized by *O*-dealkylation, like lapatinib, we detected no conjugates formed by the reaction between GSH and the quinone imine intermediate. This might be explained by the greater reactivity of the α,β-unsaturated carbonyl group of allitinib. Consequently, GSH reacted with α,β-unsaturated carbonyl group more readily than with the quinone imine group.

DMD Fast Forward. Published on March 5, 2014 as DOI: 10.1124/dmd.113.056341
This article has not been copyedited and formatted. The final version may differ from this version.



Lapatinib is suggested to be a quasi-irreversible inhibitor of CYP3A4, which is mediated by metabolites derived from *N*-oxidation (Takakusa et al., 2011). Another in vitro study showed that lapatinib is also a mechanism-based inactivator of CYP3A5, and this inactivation is mediated by quinone imine (Chan et al., 2012). These studies provide good insight into the possible mechanism of hepatotoxicity of lapatinib observed in clinical trials. To determine whether allitinib inhibits CYP because its structure is analogous to that of lapatinib and its introduced acrylamide group, in vitro enzyme induction and inhibition studies were performed. The results demonstrated that allitinib did not inhibit CYP1A2, CYP2C9, CYP2C19 or CYP2D6, but was a weak inhibitor of CYP3A4 ($IC_{50}$ ~ 100 μM with midazolam as the substrate). This level of inhibition is negligible at clinical doses. Furthermore, we observed no apparent enzyme induction. These studies suggest that, even though the α,β-unsaturated carbonyl group was introduced and a quinone imide intermediate might be formed via *O*-dealkylation, allitinib does not affect CYP enzyme activity. The probability that allitinib has a pharmacological effect on coadministered drugs via the induction or inhibition of CYP is low, even though the recommended dose of allitinib is 1000 mg t.i.d.

In conclusion, we found that O-dealkylation is an important metabolic pathway of allitinib, as it is for lapatinib. However, we also found that amide hydrolysis and dihydrodiol formation are major metabolic pathways because the reactivity of the α,β-unsaturated carbonyl group is high. Multiple enzymes including P450 and epoxide hydrolase are involved in the metabolism of allitinib, but allitinib does not induce or inhibit tested CYP enzymes, suggesting a low potential of drug-drug interaction mediated by

tested CYP enzymes in case of coadministration.

**Ackowledgments.**

We wish to thank the staff at Allist Pharmaceuticals, Inc. (Shanghai, China) for synthesizing the standard compounds; Fudan University Shanghai Cancer Center (Shanghai, China) for conducting the clinical studies; Dr. Hua Xie (SIMM) for assistance with in vitro pharmacological assays of the major metabolites of allitinib; Dr. Liang Li (SIMM) for the kind help for the NMR analysis; and Mr. Yanjun Bai and Ms. Xiuli Li (SIMM) for assistance with the permeability studies.

**Authorship contributions**

*Participated in research design*: Lin, Zhong, and Chen.

*Conducted experiments*: Lin, Xie, and Gao.

*Contributed new reagents or analytic tools*: Lin, Zhong, and Chen.

*Performed data analysis*: Lin, Zhong, Xie, Gao and Chen.

*Contributed to the writing of the manuscript*: Lin and Zhong.

**References**

Baillie TA, Cayen MN, Fouda H, Gerson RJ, Green JD, Grossman SJ, Klunk LJ, LeBlanc B, Perkins DG, and Shipley LA (2002) Drug metabolites in safety testing. *Toxicol Appl Pharmacol* **182:**188-196.

Bence AK, Anderson EB, Halepota MA, Doukas MA, DeSimone PA, Davis GA, Smith DA, Koch KM, Stead AG, Mangum S, Bowen CJ, Spector NL, Hsieh S, and Adams VR (2005) Phase I pharmacokinetic studies evaluating single and multiple doses of oral GW572016, a dual EGFR-ErbB2 inhibitor, in healthy subjects. *Invest New Drugs* **23:**39-49.

Burris HA, 3rd, Hurwitz HI, Dees EC, Dowlati A, Blackwell KL, O'Neil B, Marcom PK, Ellis MJ, Overmoyer B, Jones SF, Harris JL, Smith DA, Koch KM, Stead A, Mangum S, and Spector NL (2005) Phase I safety, pharmacokinetics, and clinical activity study of lapatinib (GW572016), a reversible dual inhibitor of epidermal growth factor receptor tyrosine kinases, in heavily pretreated patients with metastatic carcinomas. *J Clin Oncol* **23:**5305-5313.

Castellino S, O'Mara M, Koch K, Borts DJ, Bowers GD, and MacLauchlin C (2012) Human metabolism of lapatinib, a dual kinase inhibitor: implications for hepatotoxicity. *Drug Metab Dispos* **40:**139-150.

Chan EC, New LS, Chua TB, Yap CW, Ho HK, and Nelson SD (2012) Interaction of lapatinib with cytochrome P450 3A5. *Drug Metab Dispos* **40:**1414-1422.

Ehrenberg L and Hussain S (1981) Genetic toxicity of some important epoxides. *Mutat Res* **86:**1-113.

Eskens FA, Mom CH, Planting AS, Gietema JA, Amelsberg A, Huisman H, van Doorn L, Burger H, Stopfer P, Verweij J, and de Vries EG (2008) A phase I dose escalation study of BIBW 2992, an irreversible dual inhibitor of epidermal growth factor receptor 1 (EGFR) and 2 (HER2) tyrosine kinase in a 2-week on, 2-week off schedule in patients with advanced solid tumours. *Br J Cancer* **98:**80-85.

Faller TH, Csanady GA, Kreuzer PE, Baur CM, and Filser JG (2001) Kinetics of propylene oxide metabolism in microsomes and cytosol of different organs from mouse, rat, and humans. *Toxicol Appl Pharm* **172:**62-74.

Garrett TP, McKern NM, Lou M, Elleman TC, Adams TE, Lovrecz GO, Kofler M, Jorissen RN, Nice EC, Burgess AW, and Ward CW (2003) The crystal structure of a truncated ErbB2 ectodomain reveals an active conformation, poised to interact with other ErbB receptors. *Mol Cell* **11:**495-505.

Geyer CE, Forster J, Lindquist D, Chan S, Romieu CG, Pienkowski T, Jagiello-Gruszfeld A, Crown J, Chan A, Kaufman B, Skarlos D, Campone M, Davidson N, Berger M, Oliva C, Rubin SD, Stein S, and Cameron D (2006) Lapatinib plus capecitabine for HER2-positive advanced breast cancer. *N Engl J Med* **355:**2733-2743.

Gonzales AJ, Hook KE, Althaus IW, Ellis PA, Trachet E, Delaney AM, Harvey PJ, Ellis TA, Amato DM, Nelson JM, Fry DW, Zhu T, Loi CM, Fakhoury SA, Schlosser KM, Sexton KE, Winters RT, Reed JE, Bridges AJ, Lettiere DJ, Baker DA, Yang J, Lee HT, Tecle H, and Vincent PW (2008) Antitumor activity and pharmacokinetic properties of PF-00299804, a second-generation irreversible pan-erbB receptor tyrosine kinase inhibitor. *Mol Cancer Ther* **7:**1880-1889.

Gonzalez-Perez M, Gomez-Bombarelli R, Arenas-Valganon J, Perez-Prior MT, Garcia-Santos MP, Calle E, and Casado J (2012) Connecting the chemical and biological reactivity of epoxides. *Chem Res Toxicol* **25:**2755-2762.

Hooberman BH, Chakraborty PK, and Sinsheimer JE (1993) Quantitative structure-activity relationships for the mutagenicity of propylene oxides with Salmonella. *Mutat Res* **299:**85-93.

Klapper LN, Kirschbaum MH, Sela M, and Yarden Y (2000) Biochemical and clinical implications of the ErbB/HER signaling network of growth factor receptors. *Adv Cancer Res* **77:**25-79.

Lee MS, Faller TH, Kreuzer PE, Kessler W, Csanady GA, Putz C, Rios-Blanco MN, Pottenger LH, Segerback D, Osterman-Golkar S, Swenberg JA, and Filser JG (2005) Propylene oxide in blood and soluble nonprotein thiols in nasal mucosa and other tissues of male Fischer 344/N rats exposed to propylene oxide vapors-relevance of glutathione depletion for propylene oxide-induced rat nasal tumors. *Toxicol Sci* **83:**177-189.

Lin L, Gao Z, Chen X, and Zhong D (2013) Development and validation of a sensitive LC-MS/MS assay for the simultaneous quantification of allitinib and its two metabolites in human plasma. *J Pharm Biomed Anal* **86C:**49-55.

Maenpaa J, Hall SD, Ring BJ, Strom SC, and Wrighton SA (1998) Human cytochrome P450 3A (CYP3A) mediated midazolam metabolism: the effect of assay conditions and regioselective stimulation by alpha-naphthoflavone, terfenadine and testosterone. *Pharmacogenetics* **8:**137-155.

Olayioye MA, Neve RM, Lane HA, and Hynes NE (2000) The ErbB signaling network: receptor heterodimerization in development and cancer. *EMBO J* **19:**3159-3167.

Peroukides S, Makatsoris T, Koutras A, Tsamandas A, Onyenadum A, Labropoulou-Karatza C, and Kalofonos H (2011) Lapatinib-induced hepatitis: a case report. *World J Gastroenterol* **17:**2349-2352.

Rabindran SK, Discafani CM, Rosfjord EC, Baxter M, Floyd MB, Golas J, Hallett WA, Johnson BD, Nilakantan R, Overbeek E, Reich MF, Shen R, Shi X, Tsou HR, Wang YF, and Wissner A (2004) Antitumor activity of HKI-272, an orally active, irreversible inhibitor of the HER-2 tyrosine kinase. *Cancer Res* **64:**3958-3965.

Rodrigues AD (1999) Integrated cytochrome P450 reaction phenotyping - Attempting to bridge the gap between cDNA-expressed cytochromes P450 and native human liver microsomes. *Biochem Pharmacol* **57:**465-480.

Roffey SJ, Obach RS, Gedge JI, and Smith DA (2007) What is the objective of the mass balance study? A retrospective analysis of data in animal and human excretion studies employing radiolabeled drugs. *Drug Metab Rev* **39:**17-43.

Shewchuk L, Hassell A, Wisely B, Rocque W, Holmes W, Veal J, and Kuyper LF (2000) Binding mode of the 4-anilinoquinazoline class of protein kinase inhibitor: X-ray crystallographic studies of 4-anilinoquinazolines bound to cyclin-dependent kinase 2 and p38 kinase. *J Med Chem* **43:**133-138.

Takakusa H, Wahlin MD, Zhao C, Hanson KL, New LS, Chan EC, and Nelson SD (2011) Metabolic intermediate complex formation of human cytochrome P450 3A4 by lapatinib. *Drug Metab Dispos* **39:**1022-1030.

Takezawa K, Okamoto I, Tanizaki J, Kuwata K, Yamaguchi H, Fukuoka M, Nishio K, and Nakagawa K (2010) Enhanced anticancer effect of the combination of BIBW2992 and thymidylate synthase-targeted agents in non-small cell lung cancer with the T790M mutation of epidermal growth factor receptor. *Mol Cancer Ther* **9:**1647-1656.

Teng WC, Oh JW, New LS, Wahlin MD, Nelson SD, Ho HK, and Chan EC (2010) Mechanism-based inactivation of cytochrome P450 3A4 by lapatinib. *Mol Pharmacol* **78:**693-703.

Ueng YF, Kuwabara T, Chun YJ, and Guengerich FP (1997) Cooperativity in oxidations catalyzed by cytochrome P450 3A4. *Biochemistry* **36:**370-381.

Xie H, Lin L, Tong L, Jiang Y, Zheng M, Chen Z, Jiang X, Zhang X, Ren X, Qu W, Yang Y, Wan H, Chen Y, Zuo J, Jiang H, Geng M, and Ding J (2011) AST1306, a novel irreversible inhibitor of the epidermal growth factor receptor 1 and 2, exhibits antitumor activity both in vitro and in vivo. *PLoS One* **6:**e21487.

Yap TA, Vidal L, Adam J, Stephens P, Spicer J, Shaw H, Ang J, Temple G, Bell S, Shahidi M, Uttenreuther-Fischer M, Stopfer P, Futreal A, Calvert H, de Bono JS, and Plummer R (2010) Phase I trial of the irreversible EGFR and HER2 kinase inhibitor BIBW 2992 in patients with advanced solid tumors. *J Clin Oncol* **28:**3965-3972.

DMD Fast Forward. Published on March 5, 2014 as DOI: 10.1124/dmd.113.056341
This article has not been copyedited and formatted. The final version may differ from this version.



**Figure Legends**

**Fig. 1**. Q-TOF MS of allitinib under high CE in the EST+ mode (A) and tentative structures of the major fragment ions of allitinib (B). The structure of allitinib can be divided into three segments according to the fragmentation pattern.

**Fig. 2**. Metabolic profiles of pooled plasma samples at the peak (A) (2 h after the third dose on day 24) and trough (B) (4 h after the third dose on day 24) steady-state levels of allitinib after the oral administration of 1000 mg of allitinib tysolate t.i.d. for 21 days to cancer patients. Upper trace, UHPLC-UV chromatogram. Lower trace, MDF processed chromatogram.

**Fig. 3**. Metabolic profiles of pooled urine samples collected at 0–24 h after the oral administration of 1000 mg of allitinib tosylate daily in cancer patients(A) and pooled feces samples collected at Day10–11 after the oral administration of 1000 mg t.i.d. of allitinib tysolate for 21 days in cancer patients (B). Upper trace, UHPLC-UV chromatogram. Lower trace, MDF processed chromatogram.

**Fig. 4**. Proposed metabolic pathways of allitinib in humans. Allitinib is extensively metabolized in vivo by *O*-dealkylation , amide hydrolysis, 27,28-dihydrodiolation, and hydroxylation of the quinoline ring and the 3-fluorobenzyloxy moiety, combinations of above pathways, and secondary phase-II conjugation.

**Fig. 5.** Incubation of allitinib (1 μM) in recombinant human CYP enzymes in the presence of NADPH at 37 °C for 1 h. (A) Effect of recombinant human CYP enzymes on the consumption of allitinib. (B) Effect of recombinant human CYP enzymes on the formation of M1 and M10.

**Fig. 6**. Effects of incubating of allitinib (1 μM) in HLM in the presence of NADPH. Difference enzyme inhibitors, including ABT (a non-specific CYP inhibitor), α-NF (a CYP1A1/2 inhibitor), quercetin (a CYP2C8 inhibitor), sulfaphenazole (a CYP2C9 inhibitor), ticlopidine (a CYP2C19 inhibitor), quinidine (a CYP2D6 inhibitor), KET (a CYP3A4/5 inhibitor), and clomethiazole (a CYP2E1 inhibitor), were used to evaluate the relative contributions of different microsomal enzyme systems to the metabolism of allitinib. (A) Effects of CYP inhibitors on the metabolism of allitinib. (B) Effects of CYP inhibitors on the formation of M1 and M10.

**Fig. 7**. Formation of epoxide and M10 after allitinib was incubated with HLM in the presence 10, 100 or 1000 μM of valpromide, an epoxide hydrolase inhibitor.

**Fig. 8**. Incubation of 2 μM (upper trace) and 20 nM (lower trace) allitinib epoxide with HLC preparation in the presence of GSH. Extracted ion chromatograms of GSH conjugate of allitinib epoxide M23 (A and B) and dihydrodiol metabolite M10 (C and D).

**Fig. 9**. Identified metabolic processes of lapatinib (A) and allitinib (B) in humans.

**Table 1** UHPLC/Q-TOF MS data for allitinib metabolites detected in human plasma, urine, and feces

| No. | Description | m/z $[M + H]^+$ | Formula | Error (ppm) | RT (min) | Fragment ions | Matrices |
|---|---|---|---|---|---|---|---|
| M0 | Allitinib | 449.116 | $C_{24}H_{18}ClFN_4O_2$ | -4.5 | 14.0 | 340.074, 339.069, 313.054, 311.074, 305.109, 287.071, 277.107, 213.081 | P, U, F |
| M1 | *O*-Dealkylation | 341.082 | $C_{17}H_{13}ClN_4O_2$ | 3.2 | 6.1 | 305.108, 277.111 | P, U, F |
| M2 | *O*-Dealkylation + alkenes reduction | 343.094 | $C_{17}H_{15}ClN_4O_2$ | -5.7 | 6.1 | 251.095, 287.075, 279.127, 307.117 | P, F |
| M3 | O-Dealkylation + hydroxylation | 357.072 | $C_{17}H_{13}ClN_4O_3$ | -9 | 6.1 | 329.089, 321.111, 229.107 | U, F |
| M4 | *O*-Dealkylation + hydration | 359.087 | $C_{17}H_{15}ClN_4O_3$ | -11.1 | 4.9 | 329.079, 313.083, 287.068, 277.103, 251.099 | F |
| M5 | *O*-Dealkylation + alkenes to dihydrodiol | 375.084 | $C_{17}H_{15}ClN_4O_4$ | -5.6 | 3.5 | 313.052, 287.073, 251.096 | P, U, F |
| M6 | Amide hydrolysis | 395.108 | $C_{21}H_{16}ClFN_4O$ | 0.6 | 11.5 | 287.075, 286.062, 251.095 | P, U, F |
| M7 | Amide hydrolysis + hydroxylation | 411.103 | $C_{21}H_{16}ClFN_4O_2$ | 0.5 | 11.4 | 287.075, 286.062, 251.094 | P, U, F |
| M8 | *O*-Dealkylation + hydroxylation + sulfation | 437.034 | $C_{17}H_{13}ClN_4O_6S$ | 4.5 | 5.0 | 357.079, 329.095, 321.095, 303.080, 229.046 | U |
| M9 | *O*-Dealkylation + cysteine conjugation | 462.107 | $C_{20}H_{20}ClN_5O_4S$ | 14.8 | 3.6 | 341.085, 313.057, 305.098, 287.071, 277.119 | U, F |
| M10 | Alkenes to dihydrodiol | 483.123 | $C_{24}H_{20}ClFN_4O_4$ | -0.2 | 11.0 | 375.072, 374.077, 357.072, 313.048, 287.073, 251.095 | P, U, F |
| M11 | Amide hydrolysis + hydroxylation + sulfation | 491.056 | $C_{21}H_{16}ClFN_4O_5S$ | -7.1 | 7.3 | 411.120, 286.063 | P |
| M12 | *O*-Dealkylation +*N*–acetylcysteine conjugation | 504.109 | $C_{22}H_{22}ClN_5O_5S$ | -4.4 | 4.9 | 375.063, 341.080, 287.068, 251.098 | F |
| M13 | *O*-Dealkylation + glucuronide conjugation | 517.115 | $C_{23}H_{21}ClN_4O_8$ | 4.1 | 3.7 | 341.08 | P, U |
| M14 | Cysteine conjugation | 570.138 | $C_{27}H_{25}ClFN_5O_4S$ | 0 | 9.9 | 483.101, 461.117, 449.118, 432.162, 426.117, 398.072, 313.051, 287.075 | P, U, F |
| M15-1 | Amide hydrolysis + hydroxylation + glucuronide conjugation | 587.125 | $C_{27}H_{24}ClFN_4O_8$ | -15.6 | 5.8 | 411.102, 286.061 | P |
| M15-2 | Amide hydrolysis + hydroxylation + glucuronide conjugation | 587.141 | $C_{27}H_{24}ClFN_4O_8$ | 10.8 | 9.7 | 411.102, 303.061, 302.059, 267.090, 229.130 | P, U |
| M16 | *N*-Acetylcysteine conjugation | 612.153 | $C_{29}H_{27}ClFN_5O_5S$ | 7.5 | 11.0 | 449.123, 341.080, 340.085, 313.050, 311.081, 305.105, 287.063, 251.097 | U |

RT, retention time; P, plasma; U, urine; F, feces.

**Table 2** $^{1}$H-NMR data for allitinib and its major metabolites

| Position | δH, J/Hz | | | | | | |
|---|---|---|---|---|---|---|---|
| | Allitinib [a] | M1 [a] | M2 [b] | M5 [a] | M6 [b] | M10 [a] | epoxide [b] |
| 3 | 8.90, s | 8.71, s | 8.78, s | 8.44, s | 8.31, s | 8.50, s | 8.52, s |
| 6 | 7.88, d, *J* = 9.2 Hz | 7.85, d, *J* = 9.0 Hz | 7.82, d, *J* = 9.0 Hz | 7.73, d, *J* = 9.0 Hz | 7.52, d, *J* = 9.2 Hz | 7.75, d, *J* = 9.0 Hz | 7.77, d, *J* = 9.2 Hz |
| 7 | 8.07, dd, *J* = 9.1, 2.0 Hz | 8.16, dd, *J* = 9.0, 1.5 Hz | 7.92, dd, *J* = 9.1, 2.1 Hz | 7.96, dd, *J* = 8.9, 2.2 Hz | 7.73, dd, *J* = 9.1, 2.4 Hz | 7.98, dd, *J* = 9.0, 1.9 Hz | 7.90, dd, *J* = 9.1, 1.9 Hz |
| 9 | 9.10, d, *J* = 1.5 Hz | 8.94, d, *J* = 1.2 Hz | 8.94, d, *J* = 1.5 Hz | 8.60, d, *J* = 2.2 Hz | 8.04, d, *J* = 1.6 Hz | 8.64, d, *J* = 2.1 Hz | 8.70, d, *J* = 1.0 Hz |
| 13 | 7.48, m | 7.70, d, *J* = 8.1 Hz | 7.42, dd, *J* = 8.6, 2.7 Hz | 7.43, dd, *J* = 8.6, 2.4 Hz | 7.47, dd, *J* = 8.5, 2.1 Hz | 7.59, dd, *J* = 8.7, 2.5 Hz | 7.69, dd, *J* = 8.7, 1.9 Hz |
| 14 | 7.35, m | 7.25, d, *J* = 8.1 Hz | 7.04, d, *J* = 8.8 Hz | 6.95, d, *J* = 8.6 Hz | 7.30, m | 7.40, m | 7.47, d, *J* = 8.5 Hz |
| 17 | 7.85, d, *J* = 2.1 Hz | 7.75, d, *J* = 2.2 Hz | 7.71, d, *J* = 2.5 Hz | 7.73, d, *J* = 2.5 Hz | 7.30, m | 7.89, d, *J* = 2.6 Hz | 7.97, d, *J* = 1.9 Hz |
| 18 | 5.31, s | | | | 5.24, s | 5.21, s | 5.25, s |
| 20 | 7.85, d, *J* = 2.2 Hz | | | | 7.34, m | 7.30, m | 8.15, s |
| 22 | 7.11, d, *J* = 8.7 Hz | | | | 7.17, m | 7.25, d, *J* = 9.7 Hz | 7.26, d, *J* = 8.8 Hz |
| 23 | 7.20, dt, *J* = 2.2, 8.7 Hz | | | | 7.22, m | 7.05, dt, *J* = 2.4, 8.2 Hz | 7.19, dt, *J* = 2.0, 8.5 Hz |
| 24 | 7.11, d, *J* = 8.7 Hz | | | | 7.22, m | 7.15, d, *J* = 9.1 Hz | 7.11, d, *J* = 8.5 Hz |
| 27 | 6.54, dd, *J* = 17.0, 10.0 Hz | 6.54, dd, *J* = 16.8, 9.5 Hz | 2.44, q, *J* = 7.6 Hz | 4.28, t, *J* = 4.2 Hz | | 4.28, t, *J* = 4.2 Hz | 3.67, m |
| 28 | 5.88, dd, *J* = 10.0, 1.7 Hz | 5.88, dd, *J* = 9.5, 2.0 Hz | 1.14, t, *J* = 7.6 Hz | 3.89, d, *J* = 4.0 Hz | | 3.89, d, *J* = 4.0 Hz | 3.05, dd, *J* = 5.9, 4.5 Hz |
| | 6.37, dd, *J* = 17.0, 1.7 Hz | 6.48, dd, *J* = 16.8, 2.0 Hz | | | | | 2.98, dd, *J* = 6.2, 2.2 Hz |

[a] $CD_3OD$, 400 MHz.

[b] DMSO-$d_6$, 500 MHz.

M1, *O*-dealkylallitinib; M5, *O*-dealkyl-27,28-dihydrodiol allitinib; M6, metabolite of amide hydrolysis; M10, 27,28-dihydrodiol allitinib.

DMD Fast Forward. Published on March 5, 2014 as DOI: 10.1124/dmd.113.056341
This article has not been copyedited and formatted. The final version may differ from this version.



**Table 3** Pharmacokinetic characteristics of allitinib and its major metabolites following the oral administration of 1000 mg of allitinib tosylate t.i.d. for 21 days in cancer patients

| Time | Parameter | Allitinib | M6 | M10 |
|---|---|---|---|---|
| Day 1 | $AUC_{0-24}$ (h·ng/mL) | 529 ± 185 | 65.7 ± 39.6 | 372 ± 64.9 |
| | $C_{max}$ (ng/mL) | 56.8 ± 17.1 | 5.97 ± 3.70 | 35.8 ± 5.0 |
| | $t_{max}$ (h) | 3.56 ± 2.65 | 5.17 ± 2.47 | 4.50 ± 2.72 |
| | $t_{1/2}$ (h) | 6.30 ± 3.08 | 10.0 ± 4.18 | 7.07 ± 3.93 |
| Day 24 | $AUC_{0-24}$(h·ng/mL) | 933 ± 407 | 92.0 ± 36.0 | 699 ± 415 |
| | $C_{max}$ (ng/mL) | 111 ± 35 | 6.21 ± 2.92 | 59.9 ± 37.7 |
| | $t_{max}$ (h) | 2.83 ± 2.15 | 2.50 ± 1.00 | 3.16 ± 1.60 |
| | $t_{1/2}$ (h) | 6.61 ± 1.76 | 13.5 ± 2.90 | 7.28 ± 0.54 |
| | Accum. ratio | 1.76 ± 0.33 | 1.70 ± 0.94 | 1.78 ± 0.91 |

Values are means ± S.D.

$C_{max}$ is the maximum concentraion observed in day 1 or day 24 after administration of allitinib tosylate.

M6, metabolite of amide hydrolysis; M10, 27,28-dihydrodiol allitinib; $AUC_{0-24}$, area under the concentration–time curve for 0–24 h; $t_{max}$, time to the maximum concentration.

DMD Fast Forward. Published on March 5, 2014 as DOI: 10.1124/dmd.113.056341
This article has not been copyedited and formatted. The final version may differ from this version.



**Table 4** Results of in vitro pharmacological studies of allitinib and its metabolites

| Analyte | $IC_{50}$ (nM) for EGFR | $IC_{50}$ (nM) for ErbB2 |
|---|---|---|
| Allitinib | 0.263 ± 0.044 | 1.10 ± 0.40 |
| M1 | 0.773 ± 0.023 | 25.0 ± 5.0 |
| M6 | 1.600 ± 0.960 | 282 ± 84.0 |
| M10 | 0.755 ± 0.573 | 72.0 ± 13.0 |

Values are means ± S.D.

M1, *O*-dealkylallitinib; M6, metabolite of amide hydrolysis; M10, 27,28-dihydrodiol allitinib.

DMD Fast Forward. Published on March 5, 2014 as DOI: 10.1124/dmd.113.056341
This article has not been copyedited and formatted. The final version may differ from this version.



**Table 5** UHPLC/Q-TOF MS data for allitinib and its metabolites detected in human liver microsomes

| No. | Description | RT (min) | Formula | Measured $[M+H]^+$ | + NADPH | + NADPH + GSH |
|---|---|---|---|---|---|---|
| M0 | Allitinib | 14.1 | $C_{24}H_{18}ClFN_4O_2$ | 449.116 | + | + |
| M1 | *O*-Dealkylation | 6.1 | $C_{17}H_{13}ClN_4O_2$ | 341.082 | + | + |
| M5 | *O*-Dealkylation + alkenes to dihydrodiol | 3.6 | $C_{17}H_{15}ClN_4O_4$ | 375.084 | + | + |
| M6 | Amide hydrolysis | 11.6 | $C_{21}H_{16}ClFN_4O$ | 395.108 | + | + |
| M10 | Alkenes to dihydrodiol | 11.1 | $C_{24}H_{20}ClFN_4O_4$ | 483.123 | + | + |
| M14 | Cysteine conjugation | 10.0 | $C_{27}H_{25}ClFN_5O_4S$ | 570.138 | – | + |
| M22 | Glutathione conjugation | 9.7 | $C_{34}H_{35}ClFN_7O_8S$ | 756.206 | – | + |

RT, retention time; GSH, glutathione; M1, *O*-dealkylallitinib; M5, *O*-dealkyl-27,28-dihydrodiol allitinib; M6, metabolite of amide hydrolysis; M10, 27,28-dihydrodiol allitinib; M14, thiol cysteine conjugate; M22, GSH conjugate.

Fig. 1

DMD Fast Forward. Published on March 5, 2014 as DOI: 10.1124/dmd.113.056341
This article has not been copyedited and formatted. The final version may differ from this version.

A

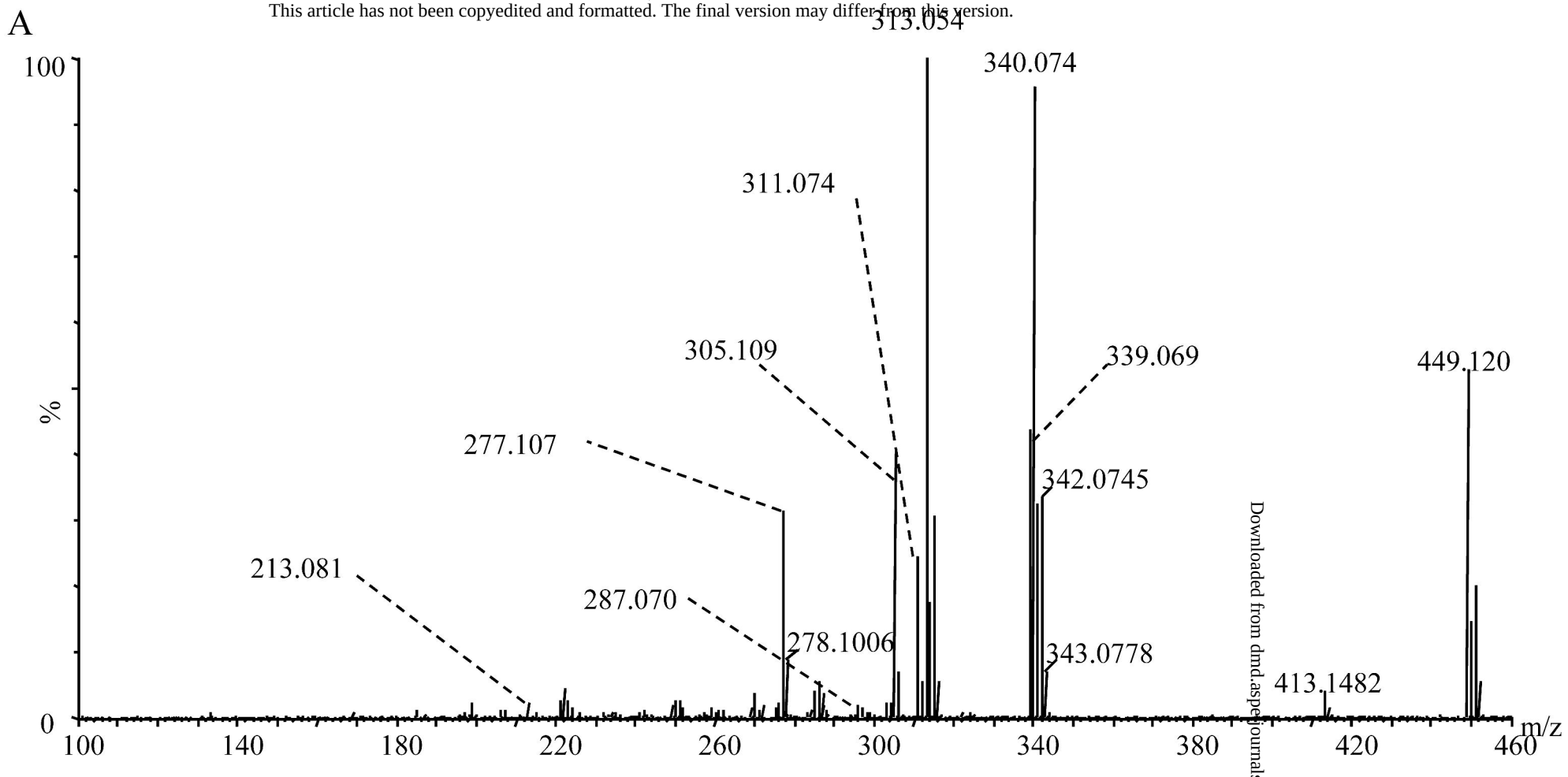




B

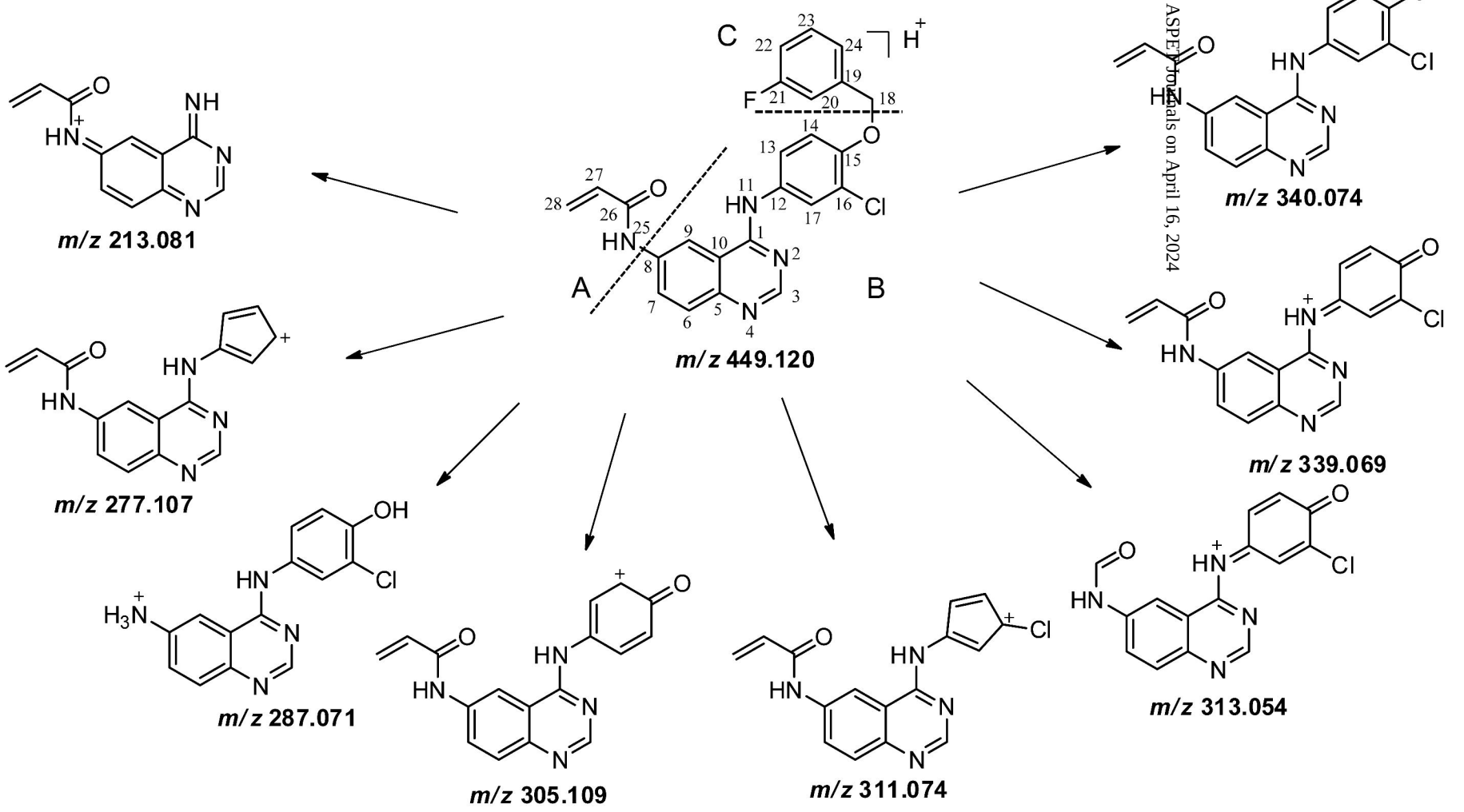

Fig. 2

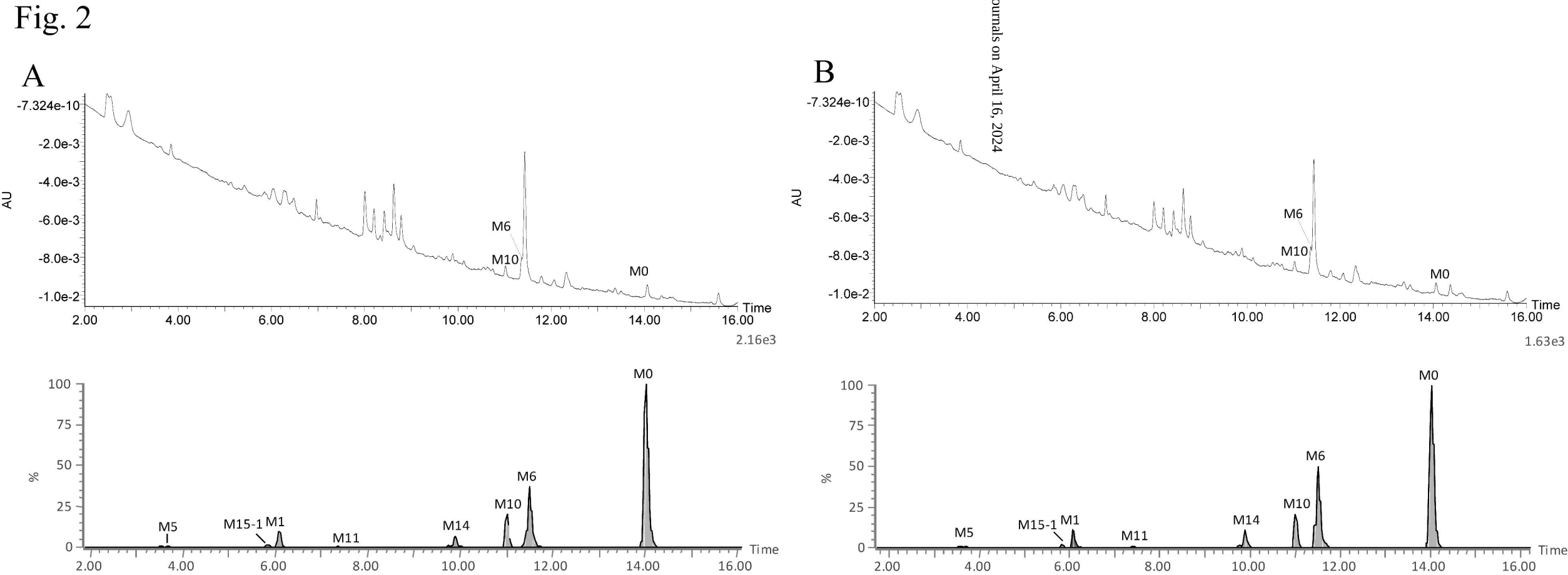

Fig. 3

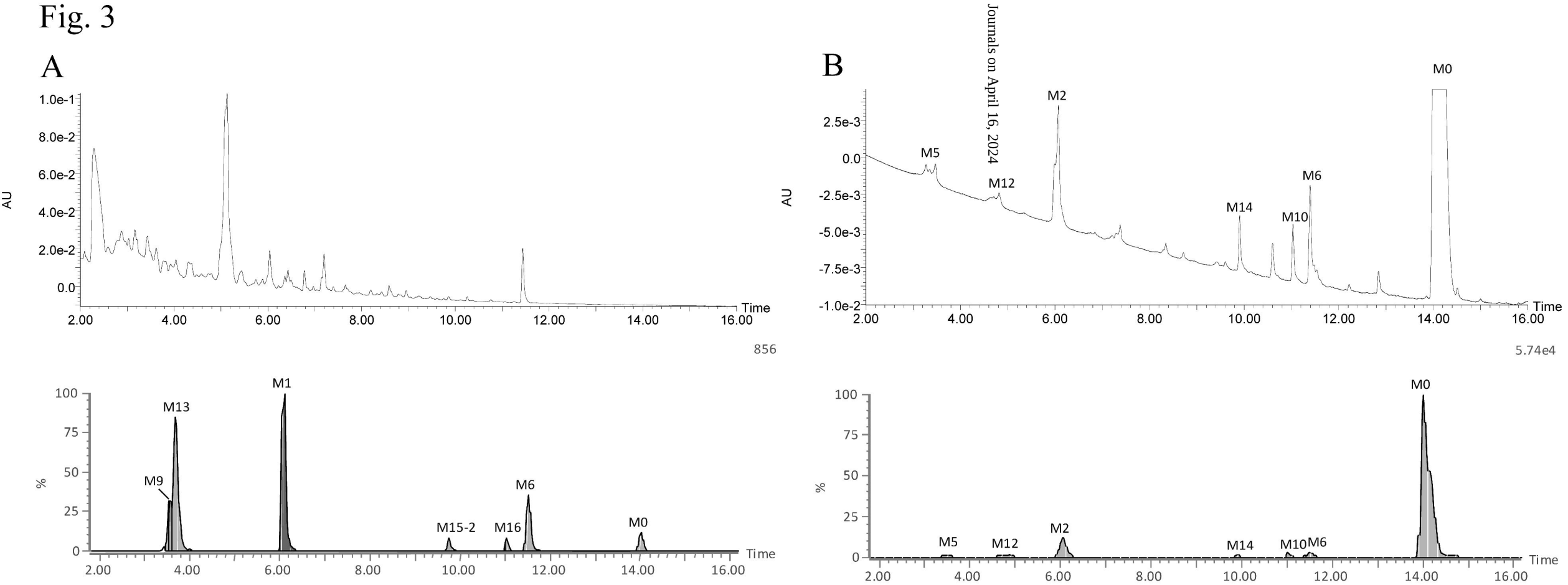
A
AU
1.0e-1
8.0e-2
6.0e-2
4.0e-2
2.0e-2
0.0
2.00
4.00
6.00
8.00
10.00
12.00
14.00
16.00
Time
856
M1
M13
M9
M6
M15-2
M16
M0
%
100
75
50
25
0
B
Journals on April 16, 2024
M0
M2
M5
M12
M14
M10
M6
2.5e-3
0.0
-2.5e-3
-5.0e-3
-7.5e-3
-1.0e-2
5.74e4

Fig. 4

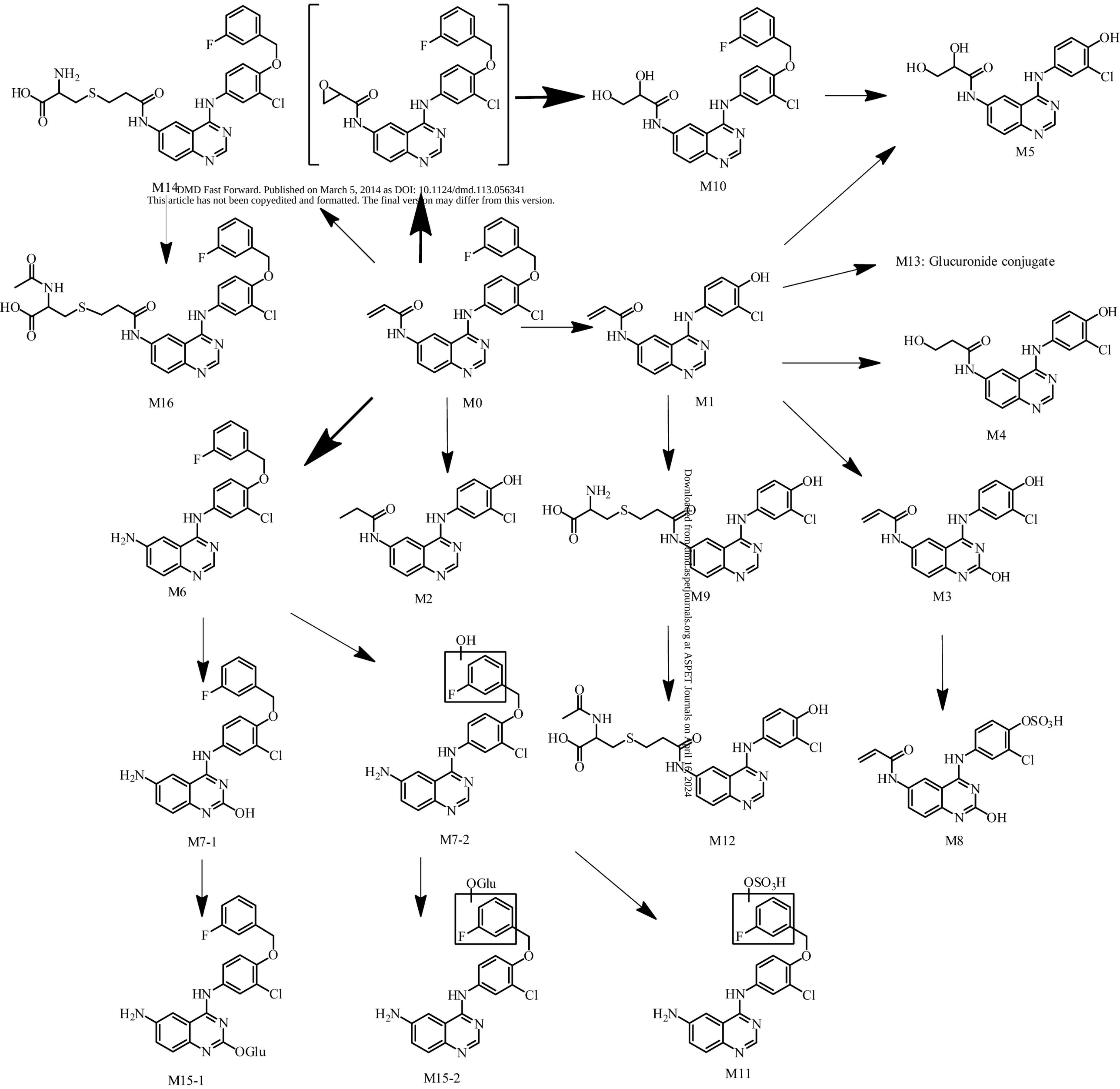

Fig. 5

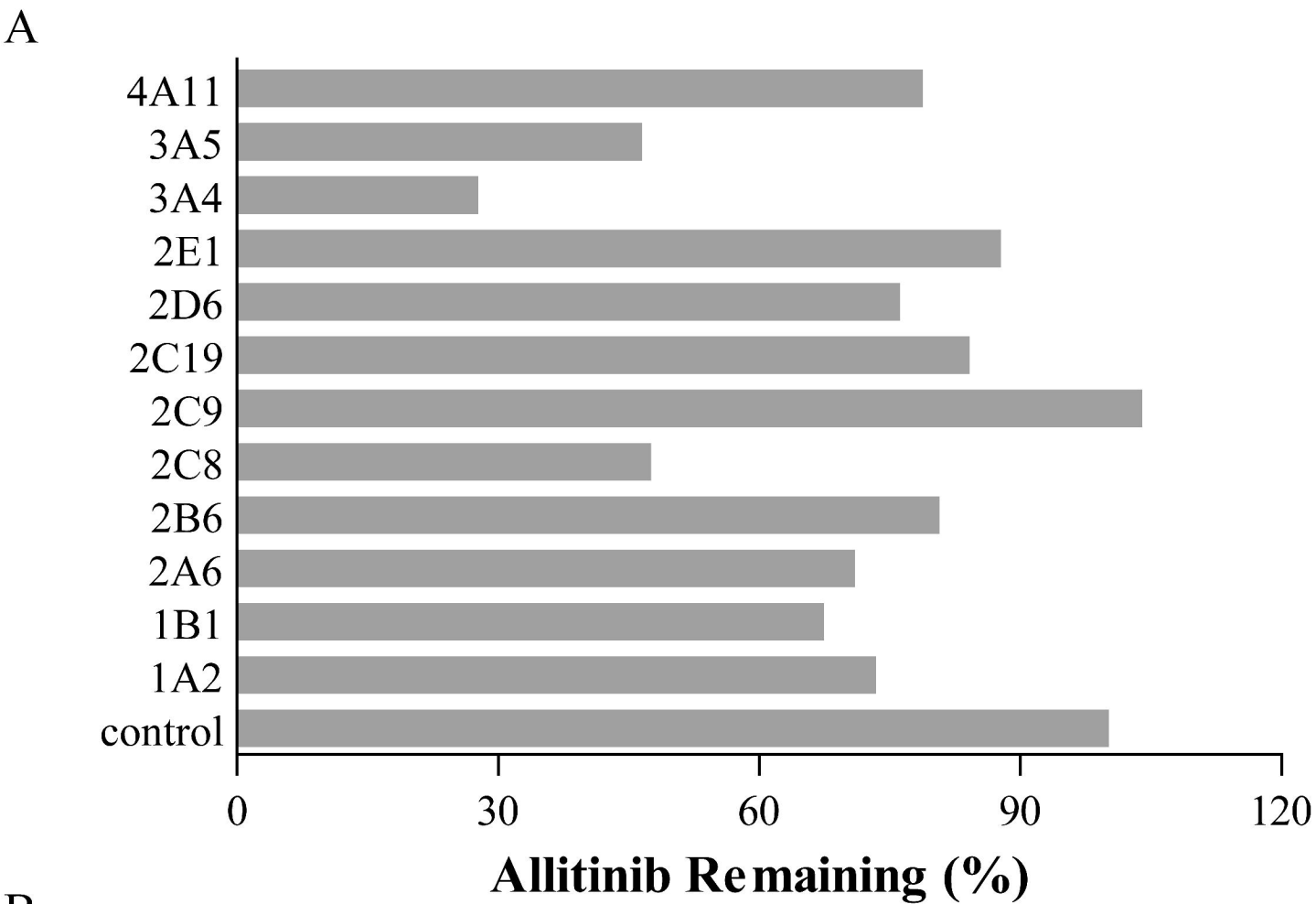


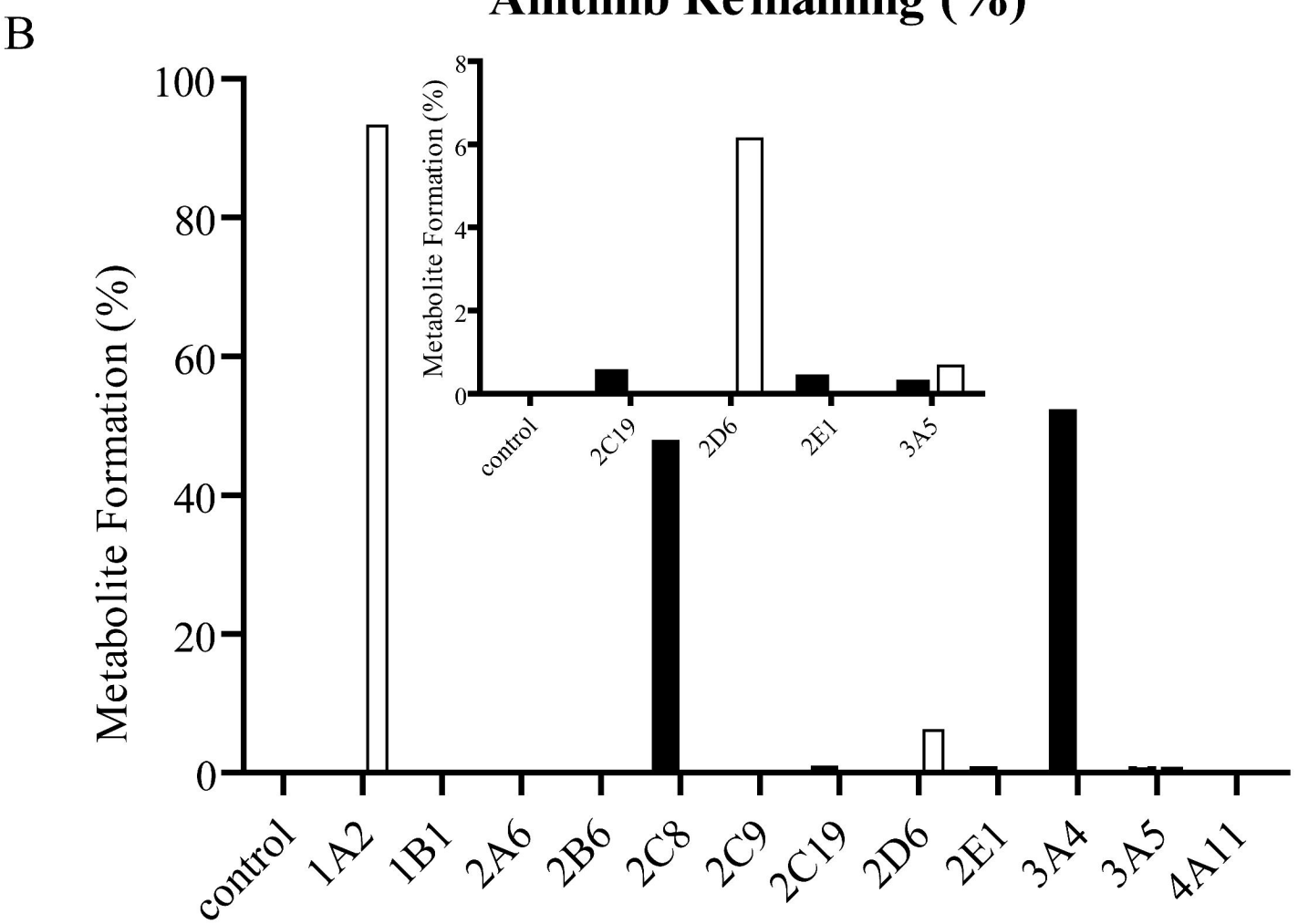

Fig. 6

A

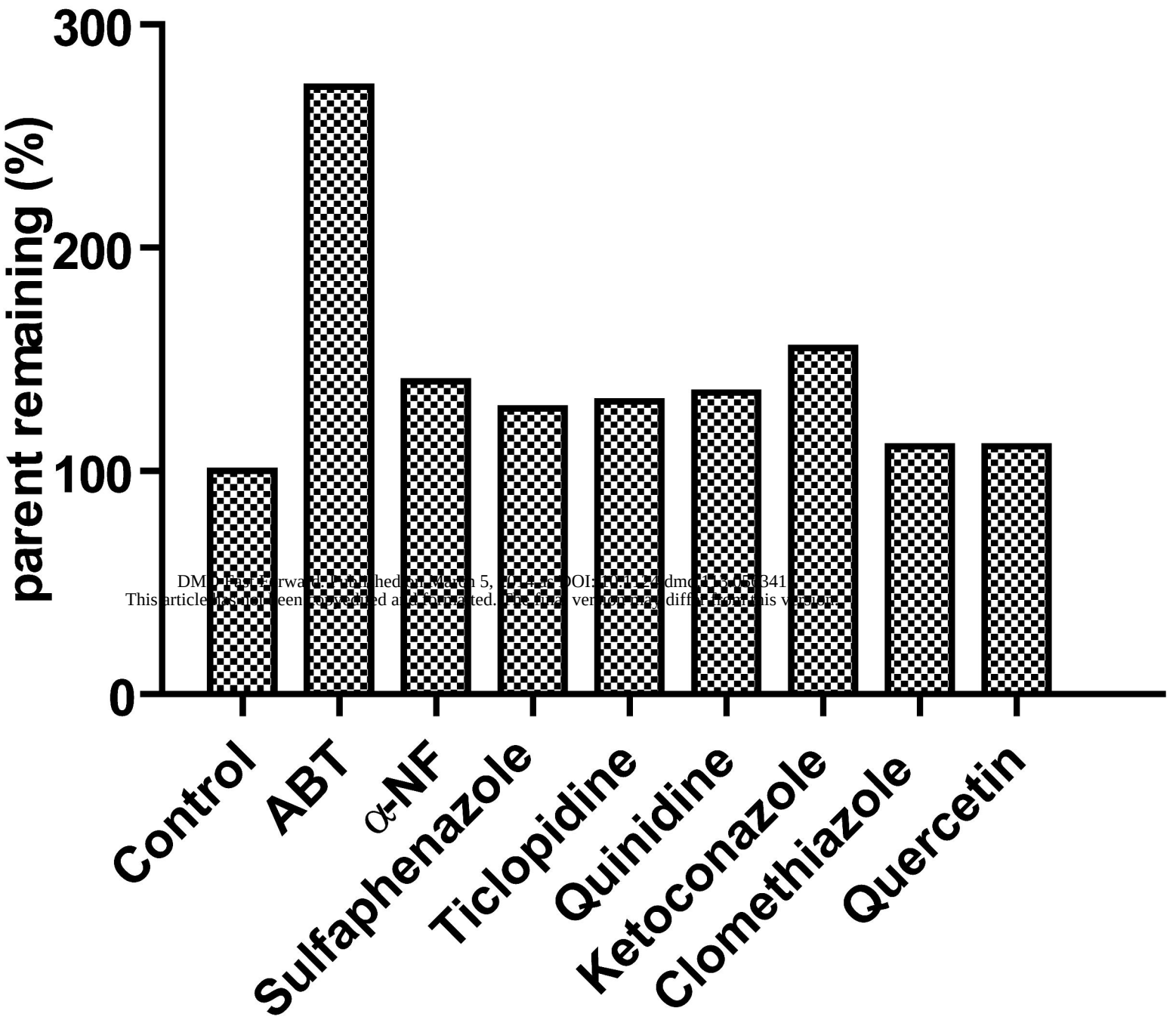




B

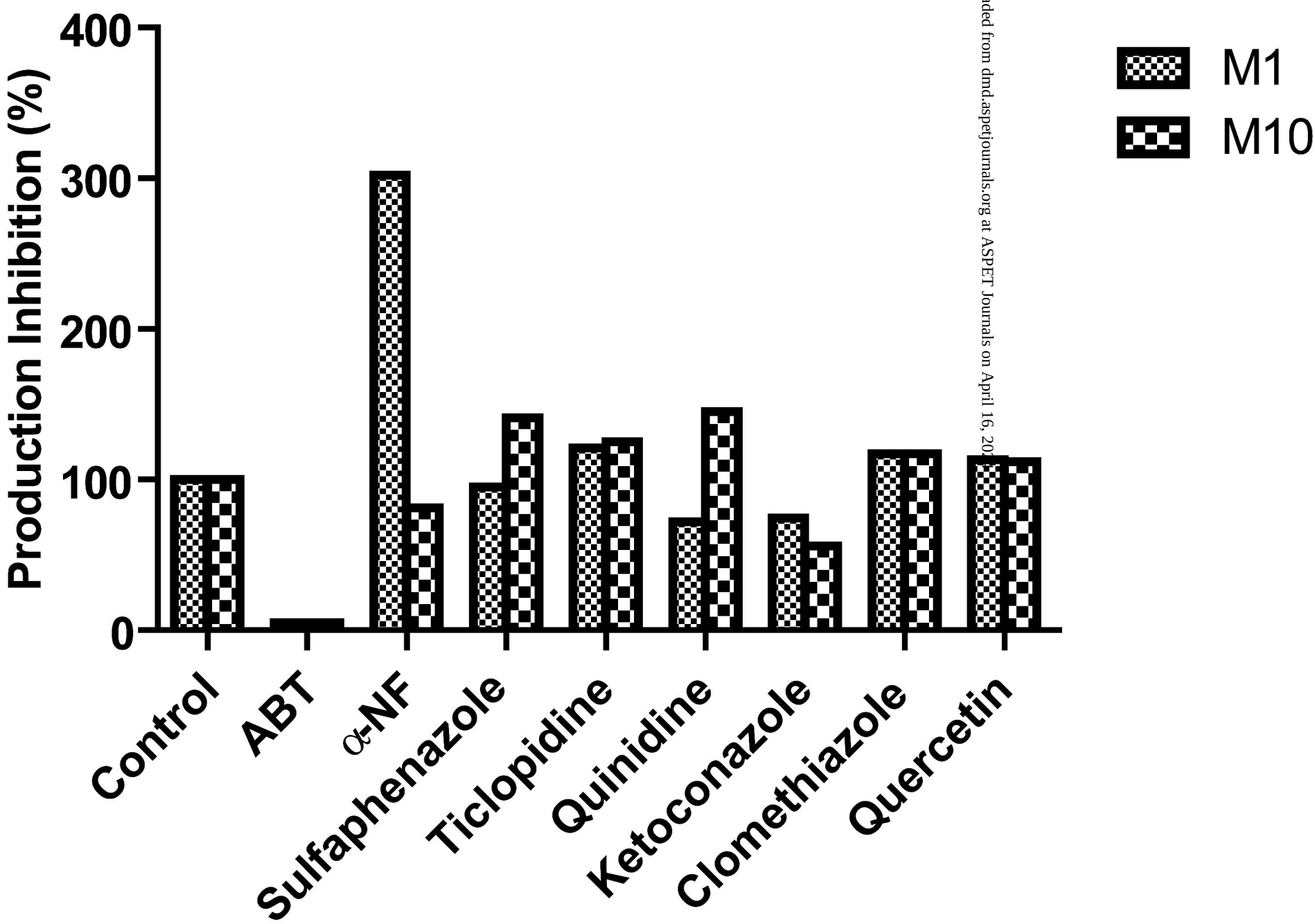

Fig. 7

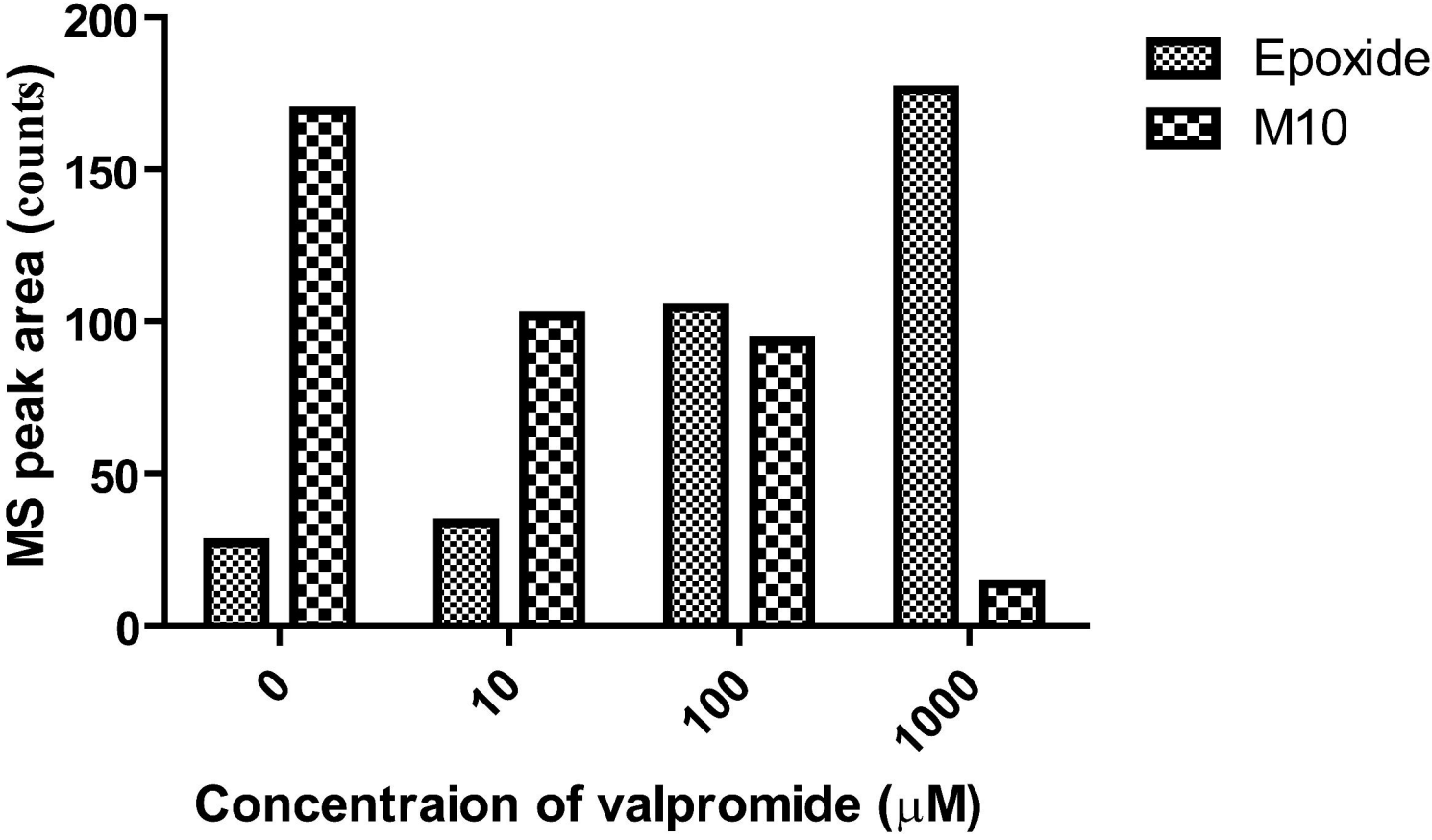
200
150
100
50
0
MS peak area (counts)
0
10
100
1000
Concentraion of valpromide (μM)
Epoxide
M10

Fig.8

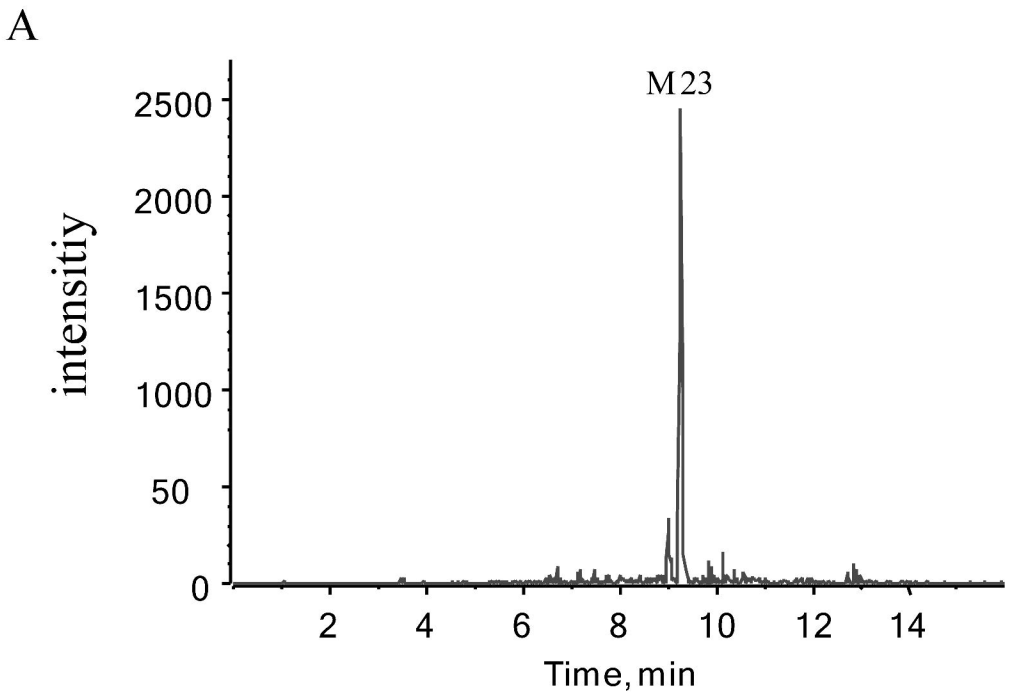


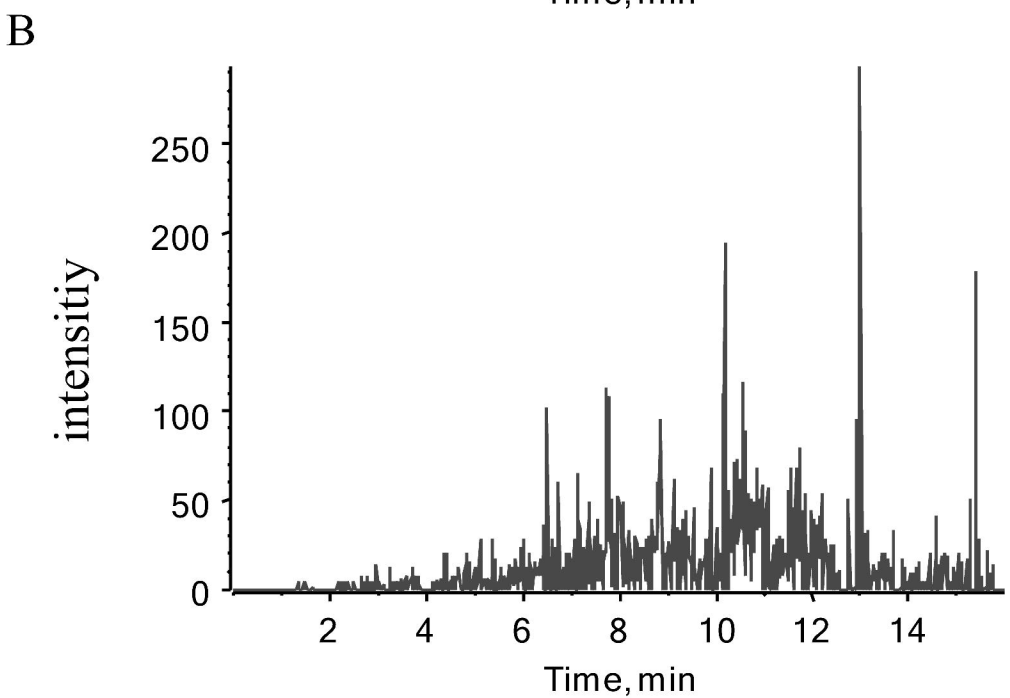


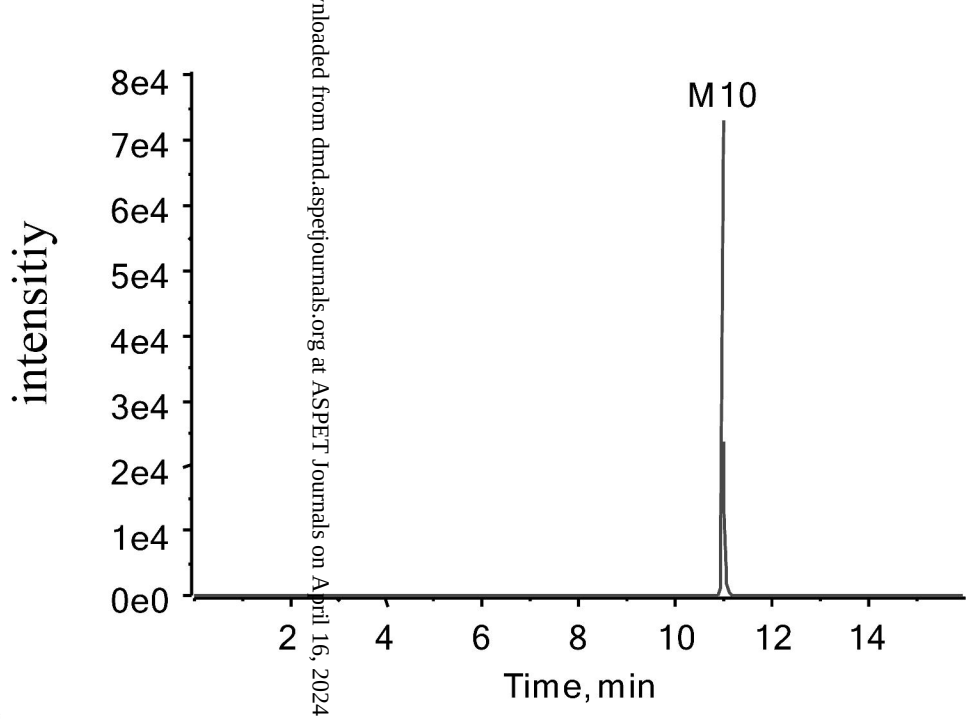


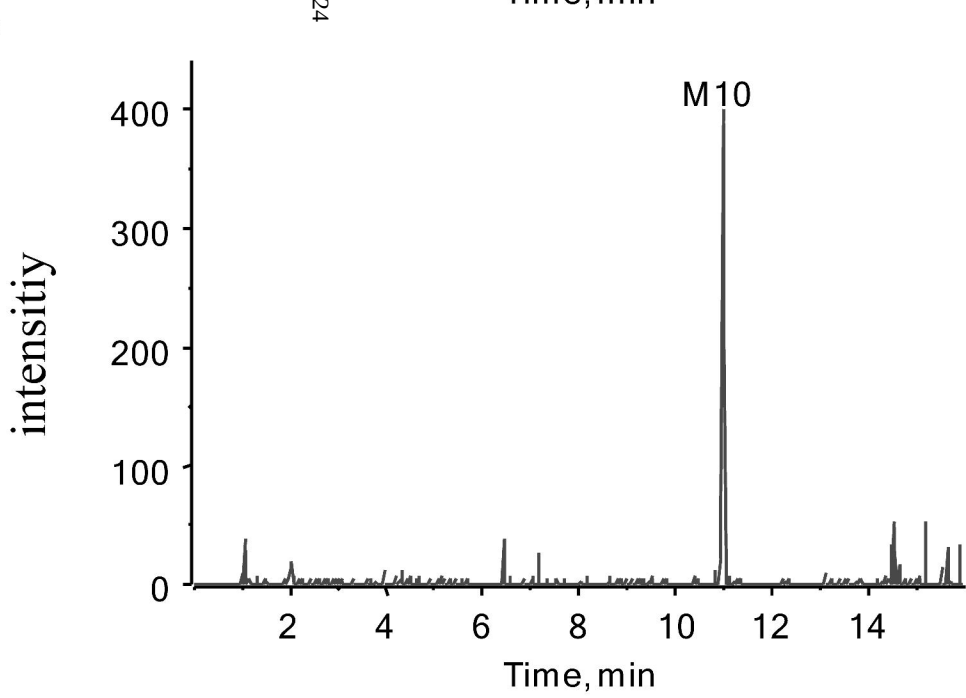

Fig.9

DMD Fast Forward. Published on March 5, 2014 as DOI: 10.1124/dmd.113.056341
This article has not been copyedited and formatted. The final version may differ from this version.

A

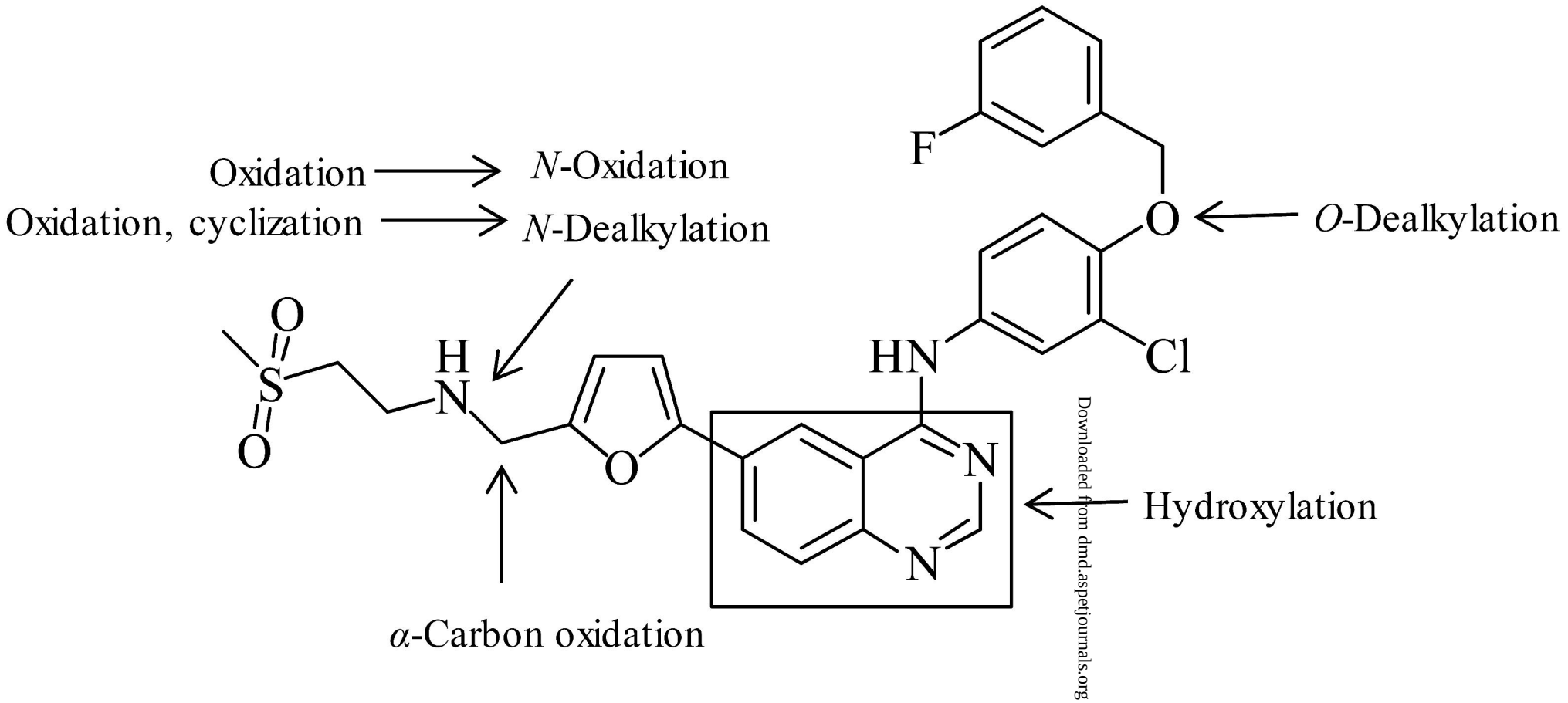




B